Monthly Notices
of the
ROYAL ASTRONOMICAL SOCIETY

MNRAS **496,** 832–850 (2020)
Advance Access publication 2020 June 3

doi:10.1093/mnras/staa1527

The SDSS/APOGEE catalogue of HgMn stars

S. Drew Chojnowski,[1★] Swetlana Hubrig,[2★] Sten Hasselquist,[3†] Rachael L. Beaton,[4] Steven R. Majewski,[5] D. A. García-Hernández[6,7] and David DeColibus[1]

[1]*Apache Point Observatory and New Mexico State University, PO Box 59, Sunspot, NM 88349-0059, USA*
[2]*Leibniz-Institut für Astrophysik Potsdam (AIP), An der Sternwarte 16, D-14482 Potsdam, Germany*
[3]*Department of Physics and Astronomy, University of Utah, 115 1400 E, Salt Lake City, UT 84112, USA*
[4]*The Observatories of the Carnegie Institution for Science, 813 Santa Barbara Street, Pasadena, CA 91101, USA*
[5]*Department of Astronomy, University of Virginia, PO Box 400325, Charlottesville, VA 22904-4325, USA*
[6]*Instituto de Astrofísica de Canarias (IAC), E-38205 La Laguna, Tenerife, Spain*
[7]*Departamento de Astrofísica, Universidad de La Laguna (ULL), E-38206 La Laguna, Tenerife, Spain*

Accepted 2020 May 8. Received 2020 May 8; in original form 2020 March 10

ABSTRACT

We report on *H*-band spectra of chemically peculiar Mercury–Manganese (HgMn) stars obtained via the SDSS/APOGEE survey. As opposed to other varieties of chemically peculiar stars such as classical Ap/Bp stars, HgMn stars lack strong magnetic fields and are defined by extreme overabundances of Mn, Hg, and other heavy elements. A satisfactory explanation for the abundance patterns remains to be determined, but low rotational velocity is a requirement and involvement in binary/multiple systems may be as well. The APOGEE HgMn sample currently consists of 269 stars that were identified among the telluric standard stars as those whose metallic absorption content is limited to or dominated by the *H*-band Mn II lines. Due to the fainter magnitudes probed by the APOGEE survey as compared to past studies, only 9/269 stars in the sample were previously known as HgMn types. The 260 newly identified HgMn stars represents a more than doubling of the known sample. At least 32 per cent of the APOGEE sample are found to be binary or multiple systems, and from multi-epoch spectroscopy, we were able to determine orbital solutions for at least one component in 32 binaries. Many of the multilined systems include chemically peculiar companions, with noteworthy examples being the HgMn+Ap/Bp binary HD 5429, the HgMn+HgMn binary HD 298641, and the HgMn+Bp Mn + Am triple system HD 231263. As a further peculiarity, roughly half of the sample produces narrow emission in the C I 16895 Å line, with widths and radial velocities that match those of the Mn II lines.

Key words: stars: chemically peculiar – stars: binaries: spectroscopic – stars: rotation.

1 INTRODUCTION

Whereas strong magnetic fields are the cause of the chemical peculiarities in classical Ap/Bp stars, the origin of the occasionally extreme heavy metal abundances in HgMn stars remains to be determined. The HgMn stars are typically defined by their optical spectra, in which overabundances of Hg (up to 6 dex over Solar; e.g. White et al. 1976) and Mn (up to 3 dex over Solar; e.g. Smith & Dworetsky 1993) are the most obvious anomalies. Modern research shows that HgMn stars actually exhibit what appears to be a steady increase of overabundance with increasing atomic number (Ghazaryan & Alecian 2016). Other elements that can be readily confirmed as overabundant using ground-based data include P, Ga, Y, Xe, Pt, and Au. At the same time, light elements such as He are typically found to be underabundant (e.g. Castelli & Hubrig 2004). Strong isotopic anomalies have been detected for the chemical elements Ca, Pt, and Hg, with the patterns changing from one star to the next (Hubrig, Castelli & Wahlgren 1999; Castelli & Hubrig 2004).

Classification of HgMn stars based solely on the presence of Hg II and Mn II lines in the optical has naturally resulted in a very narrowly defined and homogeneous sample compared to other chemically peculiar stars like the magnetic Ap/Bp stars and the (also poorly understood) metallic-lined Am/Fm stars. The HgMn stars cover a small spectral type range of B7–A0 main sequence stars (Renson & Manfroid 2009), and with an average rotational velocity of just $<v \sin i>\approx 30\,\mathrm{km\,s^{-1}}$ (maximum $v \sin i$ around $100\,\mathrm{km\,s^{-1}}$), they are slow rotators as a rule. Considering the HgMn star catalogues

★ E-mail: drewski@nmsu.edu (SDC); shubrig@aip.de (SH)
† NSF Astronomy and Astrophysics Postdoctoral Fellow.

of Schneider (1981), Renson & Manfroid (2009), and Ghazaryan & Alecian (2016), as well as more recent finds by Alecian et al. (2009), González & Levato (2009), Monier, Gebran & Royer (2015, 2016), Monier et al. (2017), Ćalıskan & Ünal (2017), Hümmerich et al. (2018), we estimate that there were 194 Galactic HgMn stars known prior to this work.

Over the past few decades it has become clear that the distributions of most or all elements on the surfaces of HgMn stars are inhomogeneous, i.e. these are stars with chemical/abundance spots. This was initially suspected by Hubrig & Mathys (1995) based on the dramatically differing strength of the Hg II 3984 Å line for binary HgMn stars with similar spectral types but different inclination angles, and it was confirmed for the first time by Malanushenko (1996), who found that the radial velocities of the He I lines of α And were variable with a period corresponding to the rotation period of the star. Recent high-resolution spectroscopic studies have subsequently shown that abundance spots on HgMn stars are the rule rather than the exception (Briquet et al. 2010; Hubrig et al. 2010; Makaganiuk et al. 2011, 2012, etc.). The spot patterns not only differ strongly from element to element, they are also highly variable, changing over time-scales as short as a few months (e.g. Korhonen et al. 2013). It is well known that in the case of Ap/Bp stars, the spot patterns are correlated with the topology of their strong, global magnetic fields. The existence of abundance spots on the comparatively non-magnetic HgMn stars is therefore quite perplexing. However, the problem may be partially resolved by the recent detection of variable, weak, tangled magnetic fields in two HgMn stars (Hubrig et al. 2020).

Another key aspect of HgMn stars seems to be their high rate of binarity/multiplicity. Based on a check of literature radial velocity and binary orbit studies, Hubrig & Mathys (1995) found that the multiplicity fraction may be as high as 67 per cent and that there was a preference for orbital periods shorter than 20 d. Schöller et al. (2010) subsequently used high-contrast imaging to detect visual companions around 28 of 56 observed HgMn stars, suggesting a multiplicity fraction of at least 50 per cent. Recently, Kervella et al. (2019) studied the multiplicity fraction of nearby stars by combining proper motions from the *Hipparcos* and *Gaia* catalogues to check for proper motion anomalies (PMa) indicative of one or more companion objects. Of the 155 HgMn stars included in the study, 60/155 are known visual multiple stars and 36 of these 60 exhibit significant PMa. Another 43 HgMn stars for which companions have not been visually identified also exhibit significant PMa, leading to a total of 103/155 (66 per cent) definite or possible multiples, consistent with the findings of Hubrig & Mathys (1995).

The companions of HgMn stars are frequently also found to be chemically peculiar. The bright HgMn binary 46 Dra is one of the more remarkable examples, since the companion is a nearly equal mass star that also shows the HgMn pecularities (Tsymbal et al. 1998). The 41 Eri, HR 7694, and HD 33647 systems are further examples of HgMn + HgMn binaries. A few systems also include magnetic chemically peculiar companions, with fields having been measured in the Am companion of χ Lup (Mathys & Hubrig 1995) and in the Ap companion of HD 161701 (Hubrig et al. 2014). The latter system is noteworthy in terms of being the only known example of an HgMn + Ap binary (González et al. 2014). More typically, the companions are found to be Am stars, especially the cooler ones (Ryabchikova 1998).

In the HgMn binaries with synchronously rotating components, the stellar surfaces facing the companion star usually display low-abundance element spots, whereas the surface of the opposite hemisphere, as a rule, is covered by high-abundance element spots (Hubrig et al. 2012). Membership in binary and multiple systems may therefore be an important clue towards developing a better understanding of HgMn stars.

The puzzling pattern of chemical abundances and variability, as well as the poorly understood role of magnetic fields in the HgMn stars challenges our very understanding of the nature of these objects. In the following, we report on the detection of 269 HgMn stars (only nine previously known) in the *H*-band spectra obtained within the framework of the SDSS/APOGEE survey. This new sample represents a more than doubling of the number of known HgMn stars, and is generally an extension of the known sample to fainter magnitudes than have been probed in past studies. In addition to analysing the *H*-band line content and line profiles of HgMn stars for the first time, we use the multi-epoch spectra available for most of the stars to measure radial velocities (RVs) and search for binaries. Where possible, we also estimate orbital parameters for the numerous single-lined (SB1), double-lined (SB2), and triple-lined (SB3) spectroscopic binaries among the sample.

2 DATA

2.1 SDSS/APOGEE *H*-band spectroscopy

The APOGEE instruments are 300-fibre, $R = 22\,500$, *H*-band spectrographs that operate on the Sloan 2.5 m telescope (Gunn et al. 2006) at Apache Point Observatory (APO, APOGEE-N) and on the Du Pont 2.5 m telescope (Bowen & Vaughan 1973) at Las Campanas Observatory (LCO, APOGEE-S). Each APOGEE instrument records most of the *H*-band (15 145–16 960 Å; vacuum wavelengths used in this paper) on three detectors, with coverage gaps between 15 800–15 860 Å and 16 430–16 480 Å (Wilson et al. 2019) and with each fibre subtending a $\sim$2 arcsec diameter on-sky field of view. The typical exposure time for an APOGEE 'field' (1.5°–3° diameter area of sky) is one hour, or roughly the time needed to reach signal-to-noise ratios (S/N) of 100 for stars with $H \le 11$ mag. The fields are usually observed multiple times on different nights, months, or years, to accumulate signal for fainter targets, and the individual spectra are later combined to produce high quality spectra for chemical abundance analysis. Majewski et al. (2017) provided a detailed overview of the APOGEE survey, and Nidever et al. (2015) described the data reduction process. This paper makes use of spectra obtained during both SDSS-III (Eisenstein et al. 2011) and SDSS-IV (Blanton et al. 2017) and reduced by the 15th SDSS data release (DR15; Aguado et al. 2019) version of the reduction pipeline.

The APOGEE targeting strategy was summarized by Zasowski et al. (2013, 2017), but some of the relevant details will be repeated here. In each APOGEE observation, 15–35 telluric standard stars (*TSS*) are targeted to facilitate removal of telluric absorption features from the science spectra. The *TSS* are selected quasi-randomly based on raw (un-dereddened) Two Micron All-Sky Survey (2MASS; Skrutskie et al. 2006) $J - K$ colour within an *H*-band magnitude range of $7.0 < H < 11.0$. There are also spatial restrictions to account for variability of the telluric absorption over the 2°–3° fields, and during SDSS-III, they were often excluded if positioned within the projected radius of an open cluster since this might induce collisions with the fibre casings of cluster science targets. In general however, the *TSS* are the combined bluest and brightest available stars in the field of view. As of 2019 July 8, a total of 33 838 *TSS* had been observed 192 545 times for an average of 5.7 spectra per star. The HgMn sample described here is culled primarily from the *TSS* sample, though with a few stars having been targeted as confirmed or candidate open cluster members during SDSS-IV. The HgMn sample at hand averages S/N = 184 per individual spectrum, such that we are firmly operating in the high-S/N regime.

2.2 APO 3.5m + ARCES optical spectroscopy

We also obtained optical spectra of 32 newly discovered HgMn stars, 15 previously known HgMn stars, and Vega using the Astrophysical Research Consortium Echelle Spectrograph (ARCES; Wang et al. 2003) on the ARC 3.5 m telescope at APO. In each exposure, ARCES covers the full optical spectrum (3500–10 400 Å) at a resolution of $R = 31\,500$. We used standard Image Reduction and Analysis Facility (IRAF[1]) echelle data reduction techniques, including 2D to 1D extraction, bias subtraction, scattered light and cosmic ray removal, flat-field correction, wavelength calibration via Thorium–Argon lamp exposures, as well as continuum normalization and merging of orders. The majority of the new HgMn stars were observed on multiple epochs in order to improve the derived orbital solutions. Exposure times were tailored to ensure S/N>100 at 4000 Å in each observation.

3 SAMPLE SELECTION

The HgMn star sample discussed in this paper was discovered among a much larger catalogue of APOGEE Chemically Peculiar (ACP) stars that currently consists of >2100 stars collectively with ∼12 800 individual spectra. Assembly of the ACP catalogue has been based primarily on detection of the Ce III lines at 15 961, 15 965, and 16 133 Å (with weaker lines occasionally present at 15 720 and 16 293 Å), as described in Chojnowski et al. (2019). These are often the strongest metallic features in the *H*-band spectra of Ap/Bp stars, and they are often the only metallic features present in the spectra of these stars. Roughly 26 per cent of the ACP sample consists of stars that do not exhibit the Ce III lines and were instead added to the catalogue due to prior classifications of chemical peculiarity in the literature.

The Ce III lines are also useful for identifying Am/Fm stars despite the 'normal star lines' (NSL), i.e. the Mg I, Si I, Fe I, C I, S I, and Al I lines that are present in the APOGEE spectra of nearly all stars with effective temperature less than ∼8000 K, always being stronger than Ce III for Am/Fm stars. Both Ap/Bp and Am/Fm stars can exhibit the NSL however, such that there is some ambiguity. Based on inspection of the spectra of the many hundred stars in the ACP catalogue with literature Ap/Bp or Am/Fm classifications, the two groups can be distinguished based on a quite simple criterion. Namely, the ratio of Ce III 15961 Å over the neighbouring blend of Ce III 15964.928 Å + Si I 15964.424 Å is always less than unity for stars classified as Am/Fm, and vice versa for those classified as Ap/Bp stars. Another equally viable classification method is to check for the presence of lines that are only detected in the spectra of Ap/Bp-classified stars. Good options for this are the Cr II and Mn II lines, with perhaps the most useful option being the set of unidentified lines (*UL*) that are often prominent in Ap/Bp star spectra and that were used for magnetic field modulus measurement in Chojnowski et al. (2019). Although we suspect the *UL* are formed by one or more rare earth elements, the associated atomic data do not exist or are not publicly available. Regardless, these lines do not appear in the spectra of Am/Fm stars.

One of the most severe outliers among the apparent Ap/Bp stars identified via Ce III detection was the well-known HgMn star HD 207857, for which the metal absorption line content is limited to Mn II and Ce III, but with the strengths of the Mn II lines more than doubling those of the Ce III lines. This revelation prompted us to search the ∼40 000 APOGEE telluric standard stars for additional objects with Mn II absorption lines. This was done by measuring equivalent widths via direct integration of the flux contained in fixed 3 Å windows centred on the two strongest Mn II lines covered (15 413 and 15 620 Å). These lines conveniently fall in portions of the spectra that are unaffected by strong airglow emission or telluric absorption features. They are also well separated from any lines that might be expected to appear in the spectra of F-type or hotter stars, such that there is minimal confusion due to blending.

The search identified almost 500 stars with potential Mn II detections, and visual inspection of the resulting spectra confirmed ∼400 stars with Mn II. Five previously known HgMn stars (HD 36662, 45975, 49606, 158704, and 182308) were included, and unlike the case of HD 207857, the only metal lines in the associated spectra are Mn II (no Ce III). Furthermore, 44 stars recovered by the search are classified as classical Ap/Bp stars in the literature, and for 40 of these, the Mn II lines are accompanied by Ce III and either Cr II, the *UL*, or both. We therefore defined the HgMn sample based on comparison of the equivalent width of the strong Mn II 15413 Å line versus the sum of equivalent widths of Ce III 15 961 and 15 965 Å, Cr II 15 370 and 15 470 Å, and the *UL* at 15 231 and 16 184 Å. This comparison is shown in the Fig. 1, with the dashed line at $y = 60$ mÅ indicating the fairly clean separation between HgMn stars and Ap/Bp stars.

The three star symbols in the extreme lower left-hand corner of Fig. 1 correspond to stars with literature Mn-peculiar classifications that did not produce the *H*-band Mn II lines in the available spectra. For Renson 3040 (A0 HgMn), the metal line content is limited to C I and Mg I, which is typical of mid–early A-type stars. For HD 51688 (B8 SiMn), no metal lines are present in the spectra. For HD 169027 (A0 Mn), Ce III 15 961 Å and Si II 16 911 Å are possibly present in lieu of the Mn II lines.

The distinctions between HgMn stars versus apparently normal stars, Ap/Bp stars, and Am/Fm stars are further emphasized in Fig. 2, which displays APOGEE spectra of two examples each of apparently normal stars, HgMn stars, Ap/Bp stars, and Am stars. HgMn stars are most similar to the Ap/Bp stars in terms of line content, but only for the HgMn stars is the line content limited to Mn II with occasional Ce III absorption and C I emission. We are not aware of any examples of Ap/Bp stars with C I in emission, but as will be discussed in Section 7, it is a common trait of HgMn stars and exotic emission line stars. The spectrum of HD 2559 in Fig. 2 demonstrates that the C I 16895 Å line is also occasionally in emission for superficially normal late-B and early-A stars.

3.1 Sample parameters

Fig. 3 presents some basic parameters of the sample, including the spatial, brightness, and temperature classification distributions. As expected, the vast majority of APOGEE HgMn stars are located near the Galactic mid-plane, having been observed in the grid of relatively high-extinction Disc fields that have been the primary focus of the APOGEE survey. The sparsity of stars below declination $\simeq -30^{\circ}$ is caused by several factors, not only limited to the later start date of APOGEE-2 observations on the Du Pont

[1] IRAF is distributed by the National Optical Astronomy Observatories, which are operated by the Association of Universities for Research in Astronomy, Inc., under cooperative agreement with the National Science Foundation.

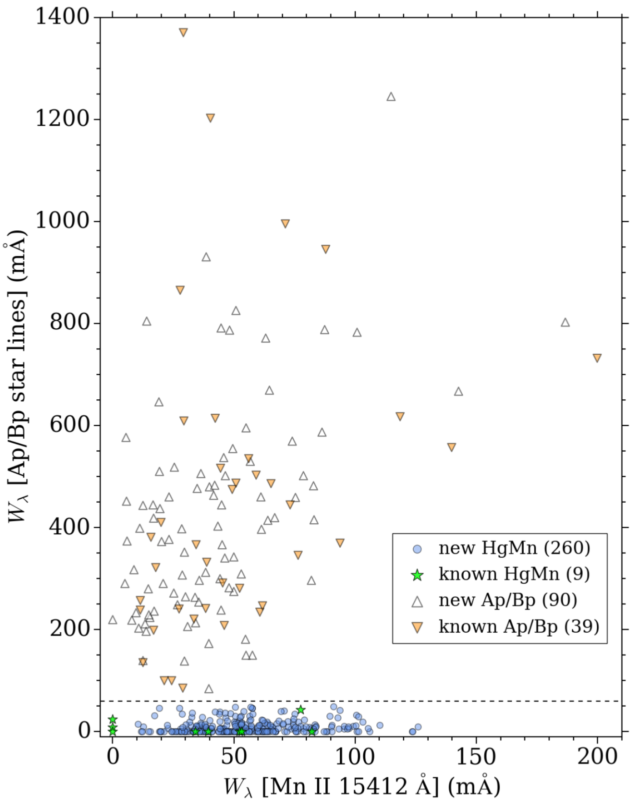

Figure 1. HgMn versus Ap/Bp classification, based on comparison of the strength of lines that typically appear in Ap/Bp star spectra to the strength of Mn II 15 413 Å. The ordinate is the sum of the equivalent widths of Ce III 15 961, 15 965, Cr II 15 370, 15 470 Å, and the unidentified lines at 15 231 and 16 184 Å (discussed in Chojnowski et al. 2019). We classify as HgMn any stars below the dashed line at $y = 60$ mÅ.

Telescope. Another factor is the fact that during APOGEE-1 and part of APOGEE-2N, 35 telluric standard stars were observed per field. Partway into APOGEE-2 however, it was decided that the telluric correction would not suffer if that number was decreased to 15. Therefore, only 15 telluric standard stars per field have been observed during some of APOGEE-2N and all of APOGEE-2S. Further, the on-sky radii of the plug-plates for APOGEE-2S are typically 0.8°, as compared to the 1.5° on-sky radii of APOGEE-2N plug-plates. The reduced field of view often leads to cooler stars being selected as telluric standard stars.

As demonstrated in the lower left-hand panel of Fig. 3, the APOGEE sample of HgMn stars is essentially an extension of the known sample to fainter magnitudes. The combined V magnitude distributions of known versus new HgMn stars suggest that many more examples should exist between $7 < V < 8$. Although a large fraction of the APOGEE HgMn sample lacks any indication of spectral type in the literature, the lower right-hand panel of Fig. 3 shows that the available spectral types are in line with expectations set by the previously known sample. With limited exceptions, the HgMn stars cover a remarkably narrow spectral type range of B7–A0.

The APOGEE HgMn star sample is summarized in Table 1, which provides for each star the 2MASS designation, an alternative identifier, the 2MASS H magnitude, the average S/N, the number of radial velocity (RV) measurements compared to the overall number of spectra, $v \sin i$, the average equivalent widths (W_λ) of Mn II 15413 Å, Ce III 15961 Å, and C I 16895 Å, the average RV, the maximum difference between individual RVs ($RV_{scat.}$), an indication of binarity, and if it exists, a literature spectral type from either SIMBAD or the chemically peculiar star catalogue of Renson & Manfroid (2009).

In the Binary Type column of Table 1, 'VIS' indicates that the star is known visual double or multiple system, 'SB1 (lit.)' indicates the star has been reported as a binary in the literature, and asterisks indicate that an orbital solution is reported in this paper (see Section 6.1). Asterisks next to the $v \sin i$ values in Table 1 indicate that $v \sin i$ was derived from optical spectra.

3.2 *H*-band linelist

Atomic data for lines that can appear in the H-band spectra of HgMn stars are given in Table 2. The Kurucz linelist[2] includes 145 Mn II lines, but only the strong lines (in terms of $\log_{10}$ of the product of statistical weight, g, and oscillator strength, f) with lower energy levels around 10 eV are detected. Although there are no Hg lines in the H-band, all of the new HgMn stars we observed in the optical exhibit Hg II, such that it is safe to say that a star whose H-band line content is limited to Mn II is almost certainly a bona fide HgMn star. The W_λ/W_{15413} column of Table 2 gives the average equivalent width ratios of the Mn II lines over Mn II 15 413 Å, based on measurements of the lines in spectra of stars with exceptionally strong Mn II. See Chojnowski et al. (2019) for a list of the empirical rest wavelengths of the *UL*.

3.3 Optical verification

Figs 4 and 5 display selected regions of the optical follow-up spectra for new and previously known HgMn stars, allowing us to verify that the new finds are indeed HgMn stars as defined in the optical. Detection of He I lines at strengths less than that of Mg II 4481 Å indicates that all of the stars fall in the B7–A0 temperature class range, as expected for HgMn stars. With the exceptions of HD 211838 and Maia, the Hg peculiarity is confirmed for all of the stars via detection of Hg II 3984 Å, which is typically the strongest Hg II line in the optical spectra of HgMn stars (Cowley & Aikman 1975). Depending on rotational velocity, dozens to hundreds of Mn II lines are readily identified in the spectra of the new HgMn stars, thus confirming the Mn peculiarity. The atlas of Castelli & Hubrig (2004) was particularly useful for identifying weak heavy metal features, and indeed many of the stars exhibit anomalously strong lines from P II, Ga II, Y II, Zr II, Xe II, Pt II, Pr III, and Nd III, all of which are known to be overabundant in HgMn stars (Ghazaryan & Alecian 2016). The stars 2MASS J02232391+5651153 and 2MASS J05542138 + 5215443 (near the bottom of Fig. 4) are perhaps the most extreme HgMn stars of our optical sample. We were able to identify ∼300 Mn II lines in the optical spectra of both stars, along with 83 P II lines and 13 Xe II lines in the spectrum of 2MASS J05542138 + 5215443.

The only stars represented in Figs 4 and 5 for which no evidence of binarity or multiplicity has been either reported in the literature or in this paper are HD 38478, 2MASS J00364423+5810121, HD 220933, and Maia. All of the new HgMn stars were targeted for optical follow-up due to being likely or definite SB1s and SB2s. For most of the stars represented in Fig. 5, the blue arrows

[2]1995 Atomic Line Data (R.L. Kurucz and B. Bell) Kurucz CD-ROM No. 23. Cambridge, Mass.: Smithsonian Astrophysical Observatory. http://kurucz.harvard.edu/lineslists/

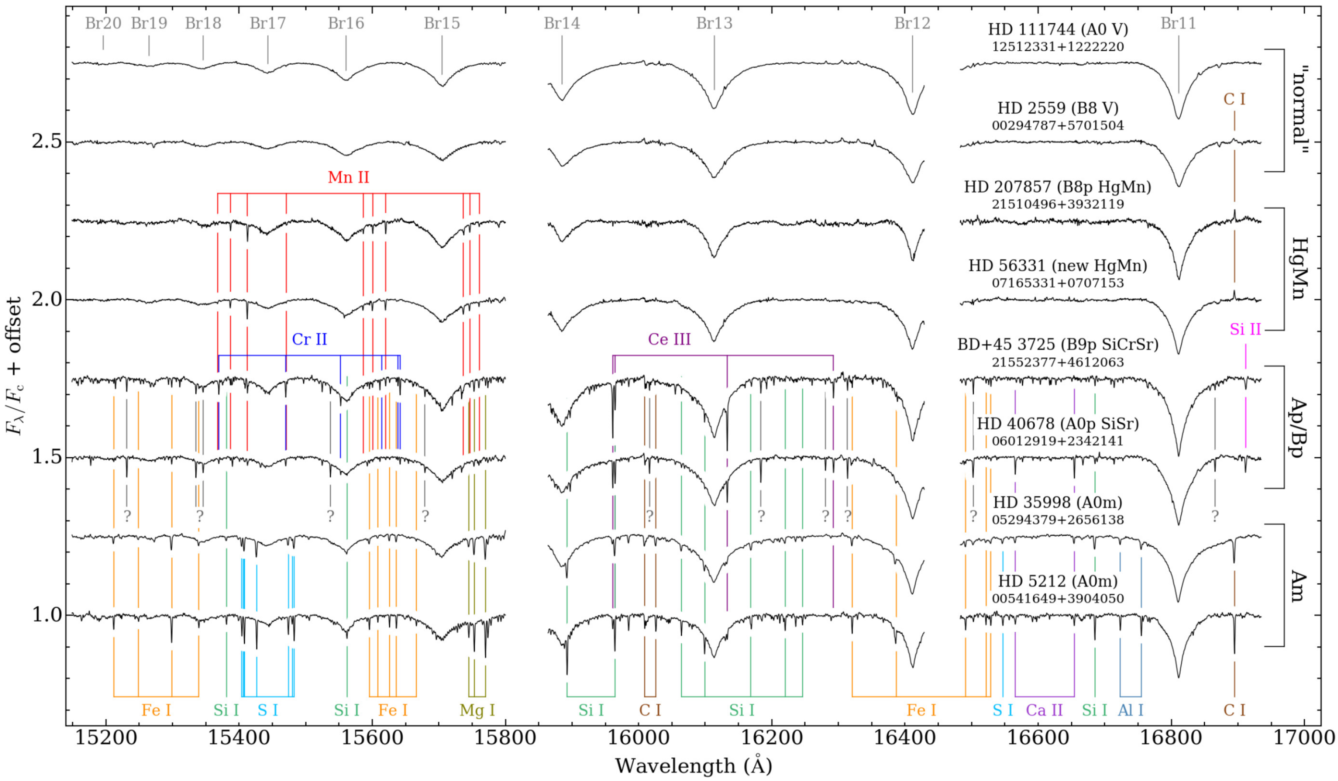

Figure 2. Comparison of the *H*-band spectra of new and previously known HgMn stars (HD 207857 and HD 56331) to presumably normal stars (HD 2559 and HD 111744), Ap/Bp stars (BD + 45 3725 and HD 40678), and Am stars (HD 35998 and HD 5212). Literature spectral types and 2MASS designations are given at right, and the majority of strong spectral features have been labelled. The line content of the normal stars is mostly limited to the hydrogen Brackett series lines, though HD 2559 exhibits weak emission in the C I 16 895 Å line. The HgMn stars have strong Mn II and emission in C I 16 895 Å. The Ap/Bp stars also have Mn II, but the strongest lines are from Ce III, Cr II, the unknown lines (labelled with question marks), Si II, and Ca II (in the case of HD 40678). The Am stars also exhibit Ce III, but the Mn II, Cr II, and unknown lines are never present. Instead, the 'normal star lines' (C I, Si I, S I, Mg I, Al I, and Fe I) are overly strong.

mark the positions of the binary companions' Mg II 4481 Å lines and occasionally also of the companions' He I 4471 Å lines. For 2MASS J06572439−0928136 and HD 158704, the companions are separated from the primaries by $<20\,\mathrm{km\,s^{-1}}$, such that the companion contributions to strong lines are thoroughly blended with the primary star lines. For α And, the companion is difficult to detect owing to the rapid rotation of both stars, so the arrows simply mark the expected companion position based on the orbit presented by Ryabchikova, Malanushenko & Adelman (1999). In the cases of the SB2 2MASS J00570626+6134007 and the SB3 2MASS J19223868+1433117, the primary and secondary stars both produce optical Mn II lines. The Mg II 4481 Å line of the tertiary in the latter system is marked with a blue arrow in Fig. 5. Most of these stars will be discussed in more detail in Section 6.

4 RADIAL VELOCITIES

Having established the HgMn sample, we proceeded to use the *H*-band Mn II lines to measure RVs by interactively fitting Gaussians to as many Mn II lines as possible from 1584/1709 APOGEE spectra (excluding some low S/N data) using the *splot* program of IRAF. From this we obtained estimates of the line centres, FWHMs, and W_λ. The line position measurements from each spectrum were averaged and a barycentric correction was added to produce the heliocentric RVs quoted in this paper. For the errors, we simply adopted the standard deviation (σ) of the line-by-line measurements. In most cases, at least two Mn II lines (usually 15413 Å and 15620 Å) were resolved in each spectrum, but in spectra where only the strongest Mn II line (15413 Å) was resolved, we assign a constant RV error of $10\,\mathrm{km\,s^{-1}}$. For the optical follow-up sample, the same process described above was applied to numerous Fe II, Si II, Cr II, Ti II, Mn II, and O I lines. The epoch-by-epoch RV measurements are provided in Table 3.

5 ROTATIONAL VELOCITIES

Rotational velocities (v sin i) were estimated based on the Gaussian full width at half-maximums (FWHMs) measured for all of the stars and a calibration derived from a sub-sample of 71 stars with particularly strong *H*-band Mn II lines ($W_{\mathrm{Mn\,II}\ 15413\ \text{Å}} > 50$ mÅ) and high-S/N spectra. The latter analysis was carried out using the IDL code *iacob broad* (Simón-Díaz & Herrero 2014), which estimates v sin i via two methods: identification of the first zero of the Fourier transform of an observed line profile, and reduction of χ^2 via a goodness-of-fit (GOF) technique whereby a theoretical line profile convolved with rotational and macroturbulent line-broadening components is compared to the observed line profile. Due to considerably more scatter in a plot of the Gaussian FWHMs versus the Fourier transform v sin i, we adopted the GOF v sin i. The upper panel of Fig. 6 shows the associated linear fit to the FWHM and GOF v sin i.

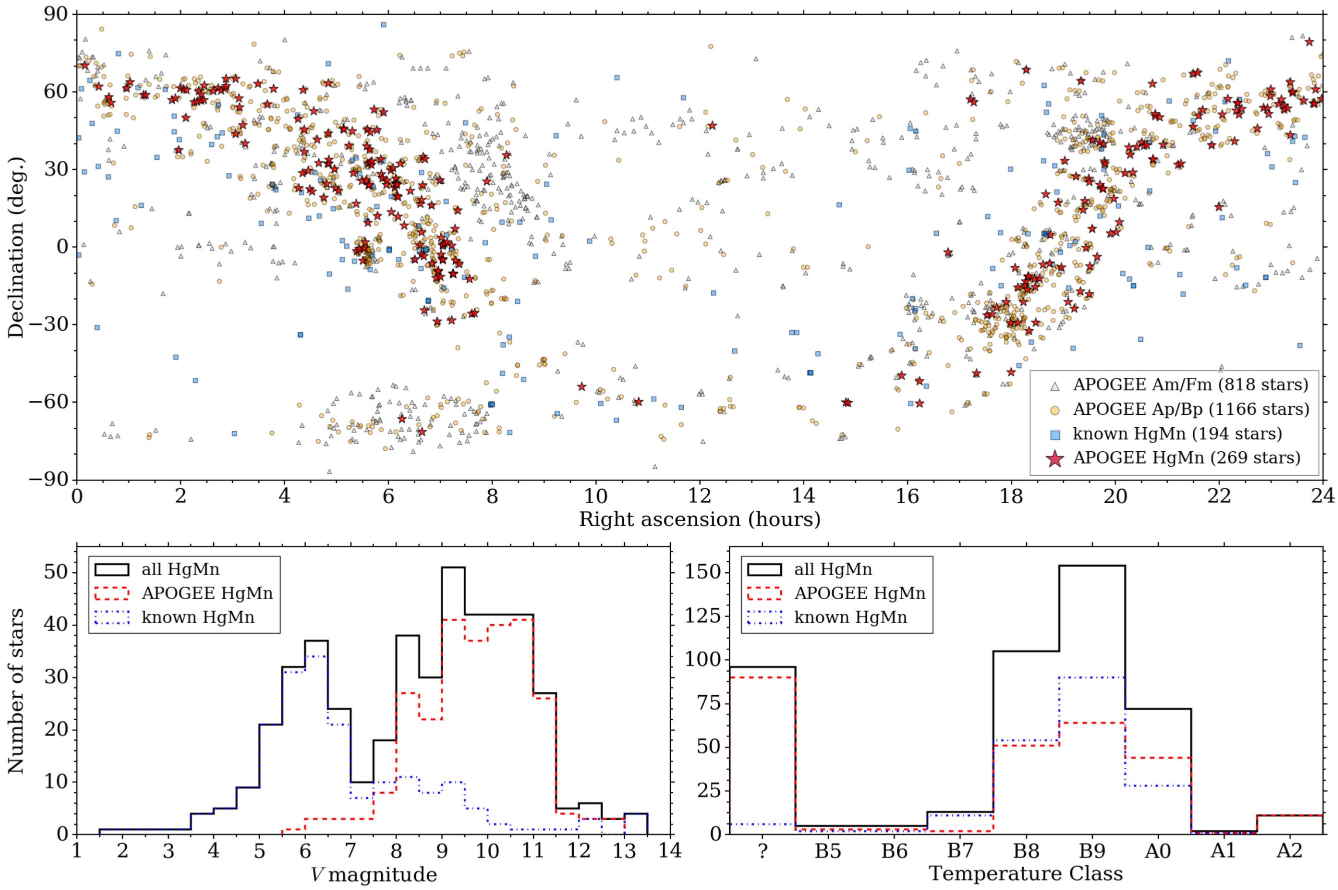

Figure 3. Top: Spatial distributions of the APOGEE chemically peculiar stars and the previously known HgMn stars. Lower left: Histogram of *V* magnitude for the HgMn stars. Lower right: Histogram of literature spectral types for the HgMn stars. The column labelled '?' in the lower right-hand panel indicates the almost 100 HgMn stars that lack a literature spectral type.

Table 1. Summary of the APOGEE HgMn sample. Only the first 10 rows are shown (full version available online).

2MASS Designation	Other Name	2MASS H (mag)	<S/N>	$N_{\rm RV}/N_{\rm obs.}$	v sin i (km s^{-1})	$<W_\lambda>$ Mn II 15413 (mÅ)	$<W_\lambda>$ Ce III 15961 (mÅ)	$<W_\lambda>$ C I 16895 (mÅ)	<RV> (km s^{-1})	RV$_{\rm scat.}$ (km s^{-1})	Binary Type	Literature Spectral Type
00091817+7022314	...	8.953	216	12/12	17 ± 8	35	...	−33	− 19.1 ± 2.1	4.7	...	...
00245787+6212255	...	10.479	112	11/12	4 ± 4	23	...	−37	− 29.5 ± 2.8	7.0	SB1	...
00364423+5810121	...	10.345	109	8/13	62 ± 2∗	61	...	...	− 31.5 ± 7.5	21.9	...	...
00390709+5558188	...	10.472	109	6/6	36 ± 7	54	...	...	− 21.5 ± 5.4	2.6	...	...
00570626+6134007	HD 5429	8.403	268	11/11	20 ± 2∗	30	...	−47	− 3.2 ± 2.2	62.5	SB2∗	B8 III[1]
01011057+6355294	Hilt 91	9.860	140	3/3	10 ± 4	82	...	−30	− 27.7 ± 1.6	0.1	...	B9 III:[1]
01165086+5902504	...	9.709	129	4/4	58 ± 5	62	...	...	− 15.5 ± 7.4	7.8	...	B8[1]
01191843+5902478	HD 7844	8.317	261	6/6	39 ± 2∗	79	...	−72	− 29.1 ± 2.0	4.3	...	B8[1]
01494647+5653549	...	10.600	88	3/3	15 ± 5	33	...	...	− 31.8 ± 6.3	5.7	...	...
01533081+5736078	...	10.507	103	3/3	37 ± 8	56	13	...	− 52.9 ± 6.4	6.7	...	...

Notes. [1]SIMBAD
[2]Renson & Manfroid (2009)

The relation between v sin i and FWHM derived from the subsample of 71 stars was then used to convert the Gaussian FWHM measurements to v sin i for the stars with weaker and/or noisier line profiles. For error estimates, the FWHM standard deviations were added in quadrature to the root mean square residual of 3.97 km s^{-1} of the liner fit in the upper panel of Fig. 6. From this, we find an average of $<v$ sin $i>$=26.8 km s^{-1} for the APOGEE sample, which is quite close to the average $<v$ sin $i>$=30.6 km s^{-1} for the previously known HgMn stars. The ranges of v sin i are also similar, going from 3 to 88 km s^{-1} for the APOGEE sample and 0–109 km s^{-1} for the known sample.

For the optical follow-up sample, we ran the *iacob broad* code on minimally blended lines that are relatively strong in the spectra of all of the stars. This included lines of Fe II (4508, 4924, 5018,

Table 2. Atomic data for lines detected in the APOGEE spectra of HgMn stars , including the hydrogen Brackett series lines (H-Br).

Ion	$\lambda_{vac.}$ (Å)	log[*gf*]	E_{lo} (eV)	E_{hi} (eV)	W_λ/ W_{15413}
Mn II	15 368.065	– 1.002	9.863	10.670	0.19
Mn II	15 387.220	– 0.272	9.864	10.670	0.51
Mn II	15 412.667	0.237	9.865	10.670	1.00
Mn II	15 470.870	– 1.869	9.007	9.809	0.12
Mn II	15 586.570	– 0.558	9.862	10.658	0.30
Mn II	15 600.576	– 0.140	9.863	10.658	0.52
Mn II	15 620.314	– 0.031	9.864	10.658	0.70
Mn II	15 737.053	– 0.303	9.862	10.650	0.50
Mn II	15 746.494	– 0.257	9.862	10.650	0.50
Mn II	15 760.789	– 0.479	9.863	10.650	0.34
Ce III	15 961.157	– 1.120	0.000	0.777	...
Ce III	15 964.928	– 1.660	0.815	1.591	...
Ce III	16 133.170	– 0.920	0.388	1.156	...
C I	16 895.031	0.568	9.003	9.736	...
H-Br20	15 196.005	– 1.489	12.749	13.564	....
H-Br19	15 264.717	– 1.416	12.749	13.564	....
H-Br18	15 345.991	– 1.339	12.749	13.564	....
H-Br17	15 443.148	– 1.256	12.749	13.564	....
H-Br16	15 560.708	– 1.167	12.749	13.564	....
H-Br15	15 704.960	– 1.071	12.749	13.564	....
H-Br14	15 884.888	– 0.966	12.749	13.564	....
H-Br13	16 113.721	– 0.852	12.749	13.564	....
H-Br12	16 411.681	– 0.725	12.749	13.564	....
H-Br11	16 811.117	– 0.582	12.749	13.564	....

5169 Å), Mn II (4479, 4756, 5559, 5571 Å), Si II (4128, 4131, 6347 Å), and O I (7772, 7774, 7775 Å). The average GOF $v \sin i$ results are plotted in the lower panel of Fig. 6 against either the $v \sin i$ estimated from APOGEE spectra or else a literature value in the cases known HgMn stars which were not observed by APOGEE. The agreement is quite good, to within 5 km s^{-1} in most cases. Due to the higher resolution and vastly greater number of available lines of the optical versus *H*-band spectra, Table 1 reports the $v \sin i$ measured from optical spectra for the optical follow-up sample.

6 MULTIPLICITY

HgMn stars are frequently or perhaps always member of binary or multiple star systems (e.g. Dolk, Wahlgren & Hubrig 2003; Schöller et al. 2010), and the APOGEE sample is no different. This is demonstrated in the upper panel of Fig. 7, which plots the maximum difference between individual RVs (RV_{scat}) versus $v \sin i$. Since it is possible for chemical spotting to make the line centres vary over the course of a rotational period, leading to measurable RV variability, we conservatively classify as definite binaries or multiples the stars for which RV_{scat} exceeds $v \sin i$ and/or the stars that are clear SB2s. We also make an exception for 2MASS J05400356 + 3153578 since a convincing SB1 orbital solution was found. Although we did not find RV variability that exceeds $v \sin i$ for the previously known HgMn stars HD 45975 and HD 207857, long-period binarity has been reported by Andrews, Chanamé & Agüeros (2017) and Pourbaix et al. (2004), respectively. These stars are represented by square symbols in Fig. 7. The stars represented by downward-facing triangle symbols in Fig. 7 are known visual doubles that we did not classify as binaries based on the APOGEE spectra.

In addition to the above SB1 classification criteria, we visually examined all available spectra to check for evidence of lines with RV offsets compared to the Mn II lines. A total of 19 SB2 systems were

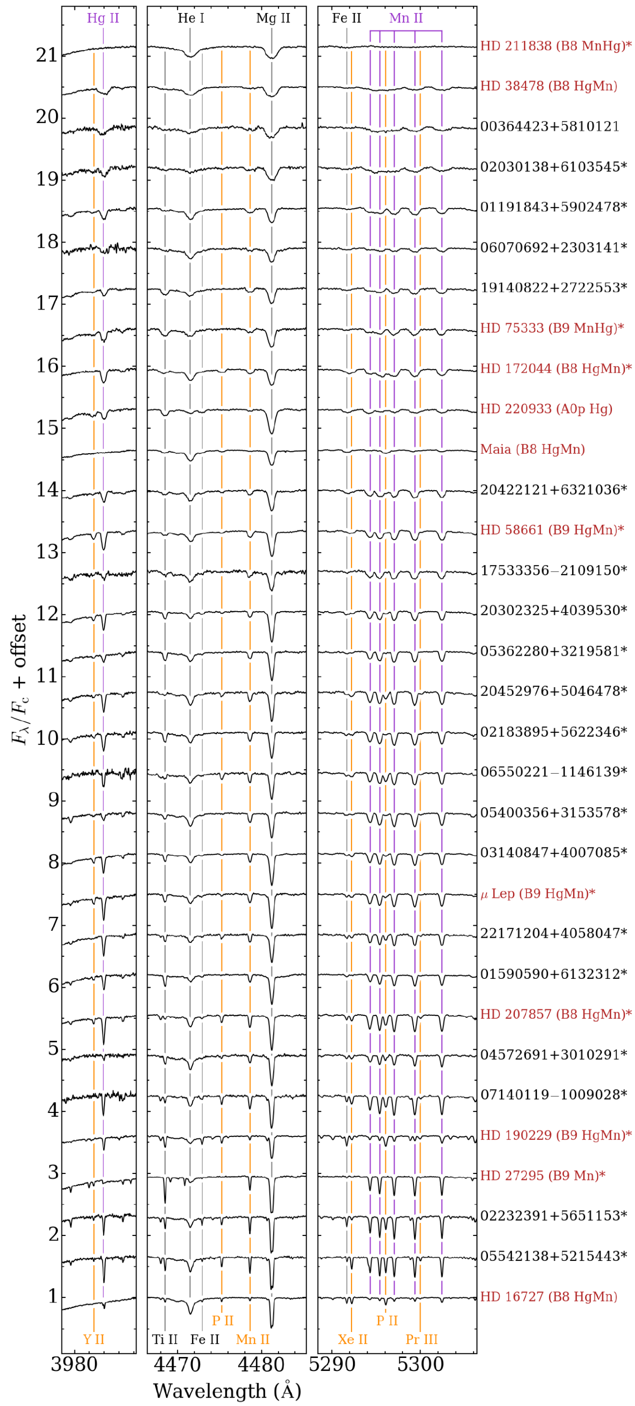

Figure 4. Optical spectra of SB1 and apparently single HgMn stars, showing regions centred on Hg II 3984 Å, He I 4471 Å, and Mg II 4481 Å, and the Mn II lines between 5294 and 5302 Å. The spectra are sorted vertically by $v \sin i$, going from 66 km s^{-1} for HD 211838 down to 2.8 km s^{-1} for HD 16727. Star names and 2MASS designations are given for the known and new HgMn stars, respectively, with literature spectral types given for the known HgMn stars and with asterisks indicating stars that are definite or suspected binaries. The grey vertical lines indicate features that appear in the spectra of normal B7–A0 stars, while purple and orange vertical lines indicate features that only appear in the spectra of chemically peculiar stars.

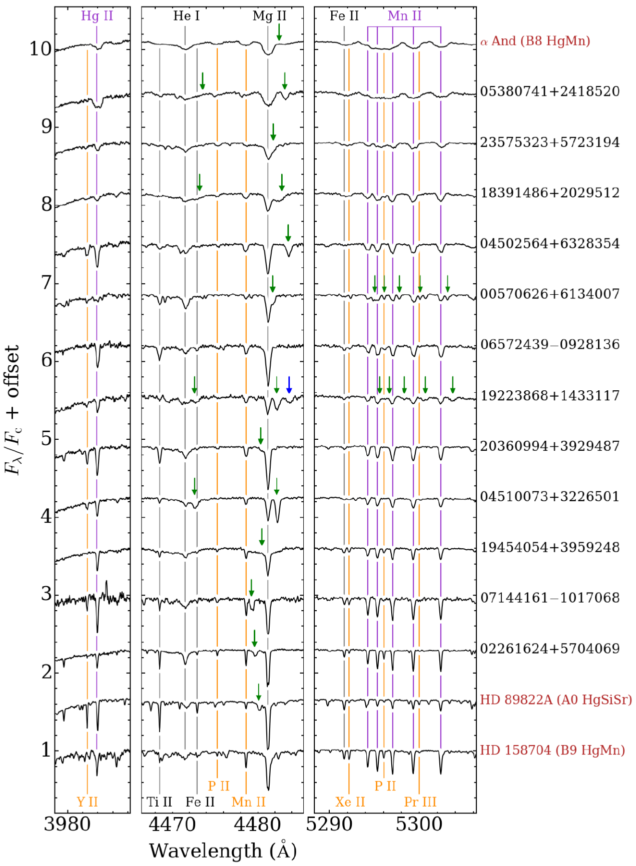

Figure 5. The same as Fig. 4 but for binary systems identified as multilined in either the optical or *H*-band. The small green arrows mark lines from the secondary stars in cases of >20 km s^{-1} velocity separations of the components, and in the case of the SB3 2MASS J19223868 + 1433117, a blue arrow marks the Mg II 4481 Å line of the tertiary star.

found based on the APOGEE data alone, including two systems that exhibit spectral lines from at least three stars (SB3s). Another four systems were confirmed as SB2s based on optical spectra, despite the companion stars not being detected in the APOGEE spectra.

Considering the 40 SB1 systems, 23 SB2s and SB3s, 11 visual double stars, and 2 previously known binaries, compared to the 165 stars whose RVs are not variable to within the projected $v \sin i$, we arrive at very conservative multiplicity fraction estimate of $N_{\rm multiples}/N_{\rm total}$ = 31 per cent (76 total multiples). However, due to the numerous stars for which the APOGEE observations were too few and/or over too short time-scales for detecting anything but very short-period binaries, 31 per cent is firmly a lower limit on the multiplicity fraction. As shown in the lower panel of Fig. 7, the fraction increases towards longer observational baselines and/or more spectra, with for example the fraction being 18 per cent for baselines shorter than 1.5 yr and 44 per cent for baselines longer than 1.5 yr. Likewise, the multiplicity fraction is 19 per cent for stars with five or fewer spectra, but it rises to 36 per cent for stars with more than five spectra. Further observations of this sample will undoubtedly reveal numerous additional binaries/multiples, particularly those with long orbital periods.

It is important to note that the sample also includes several stars that we classify as possibly single despite many APOGEE spectra taken over relatively long time-scales. The star 2MASS J19451699+2237253 (HD 344908, B8) is perhaps the best example, having been observed 38 times over a period of ∼7.8 yr. Compared to the majority of the sample, this star's Mn II lines are quite strong and narrow, such that there is minimal uncertainty about the RVs. The maximum RV difference between epochs for this star is just 3.7 km s^{-1}, implying that if a binary companion does exist, the orbital period is necessarily quite long or the companion mass quite low.

6.1 Binary orbital solutions

In the cases of RV-variable stars with at least six RV measurements, we attempted to determine Keplerian orbital parameters using the IDL code *rvfit* (Iglesias-Marzoa, López-Morales & Jesús Arévalo Morales 2015). This code utilizes an Adaptive Simulated Annealing algorithm to determine orbital parameters for both SB1s and SB2s given inputs of heliocentric Julian dates (HJD), RVs, and RV errors. For SB1s, the code outputs seven parameters including the orbital period (P), time of periastron passage (T_P), orbital eccentricity (e), the argument of the periastron (ω), the systemic radial velocity (γ), the radial velocity semi-amplitude of the primary star (K_1). These parameters can then be used to determine the mass function ($f(m)$) and semimajor axis of the primary ($a_1 \sin i$). For SB2s, the radial velocity semi-amplitude of the secondary star (K_2) is another output, allowing for calculation of semimajor axes ($a_{1,2} \sin i$, $a \sin i$), dynamical masses ($M_{1,2} \sin i^3$), and the mass ratio ($q = M_2/M1$). Any of the output parameters from *rvfit* can be fixed to a particular value or constrained by upper and lower limits in an input configuration file. In all cases we began with very loose parameter constraints and with e as a free parameter, but in cases where the value of e became comparable to its error, we forced circular orbits by setting $e = 0$. Since T_P is undefined for circular orbits, we instead provide an epoch of maximum RV ($T_{\rm max.\,RV}$) regardless of e.

Orbital solutions for 21 SB1 systems and for at least one component in 11 SB2 and SB3 systems are presented in Figs 8 and 9, with open symbols pertaining to RVs measured from APOGEE spectra and filled symbols pertaining to RVs measured from optical spectra. The periods range from 4 to 338 d, with only six systems having periods longer than 50 d. Non-zero eccentricities are found in 15 cases, led by the $e = 0.72$ of the SB1 2MASS J03140847+4007085.

The minimum number of RV measurements for which we were able to find a reasonable orbital solution was six in the cases of the SB1s 2MASS J07140119-1009028, 2MASS J16462850-0154589, and 2MASS J17533356-2109150, and for the SB2 2MASS J07144161-1017068. Only for 2MASS J07144161-1017068 is the solution stable however, thanks to a group of five APOGEE spectra separated by just 63 d. For 2MASS J16462850-0154589, numerous periods between 6 and 60 d are just as reasonable as the result shown in Fig. 8, and the orbit may also be slightly eccentric. For 2MASS J17533356-2109150, another common solution beyond the one shown in Fig. 8 has P = 171 d. The orbits of these stars will likely be revised by additional observations.

The full orbital parameters of the SB systems presented in Figs 8 and 9 are given in Tables 4 and 5.

6.2 Binary companions

The majority of the *H*-band-detected companions were evident in the *NSL* (namely, C I, Mg I, Si I, and occasionally S I), but not in the Ce III lines, indicating that they are either A or Am stars (see the Am star spectra in Fig. 2). As these stars are significantly fainter than the HgMn primaries, the features are typically quite weak,

Table 3. Radial velocity data. Only the first 10 rows are shown (full version available online).

2MASS Designation	HJD 2.45E5 +	Inst.	RV_1 ($km\,s^{-1}$)	RV_2 ($km\,s^{-1}$)	RV_3 ($km\,s^{-1}$)
00091817+7022314	5850.780	APOGEE	-19.75 ± 1.00	...	...
00091817+7022314	5851.758	APOGEE	-19.77 ± 1.00	...	...
00091817+7022314	5869.680	APOGEE	-16.80 ± 1.29	...	...
00091817+7022314	5871.698	APOGEE	-17.28 ± 1.94	...	...
00091817+7022314	6173.835	APOGEE	-21.26 ± 2.10	...	...
00091817+7022314	6204.755	APOGEE	-20.20 ± 2.75	...	...
00091817+7022314	6224.689	APOGEE	-19.50 ± 1.11	...	...
00091817+7022314	6233.644	APOGEE	-16.61 ± 4.32	...	...
00091817+7022314	6234.656	APOGEE	-18.24 ± 1.00	...	...
00091817+7022314	6257.552	APOGEE	-19.05 ± 1.57	...	...

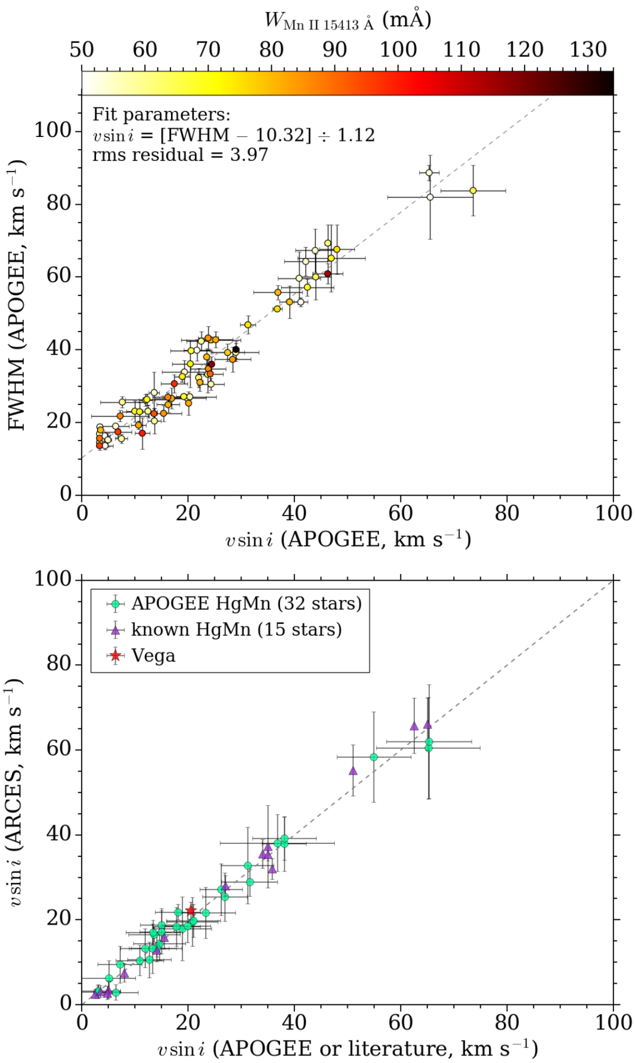

Figure 6. Top: A linear fit to the relation between goodness-of-fit v sin i results from the *iacob broad* code versus Gaussian FWHMs of the same lines. Both quantities are the averages of multiple Mn II lines, and the points are coloured by the equivalent width of Mn II 15413 Å. Bottom: A comparison of v sin i measured from our optical spectra versus v sin i from the *H*-band data or the literature, with a dotted line at $y = x$. For the previously known-but-not-observed-by-APOGEE-stars (purple triangles), the abscissa gives a literature v sin i estimate.

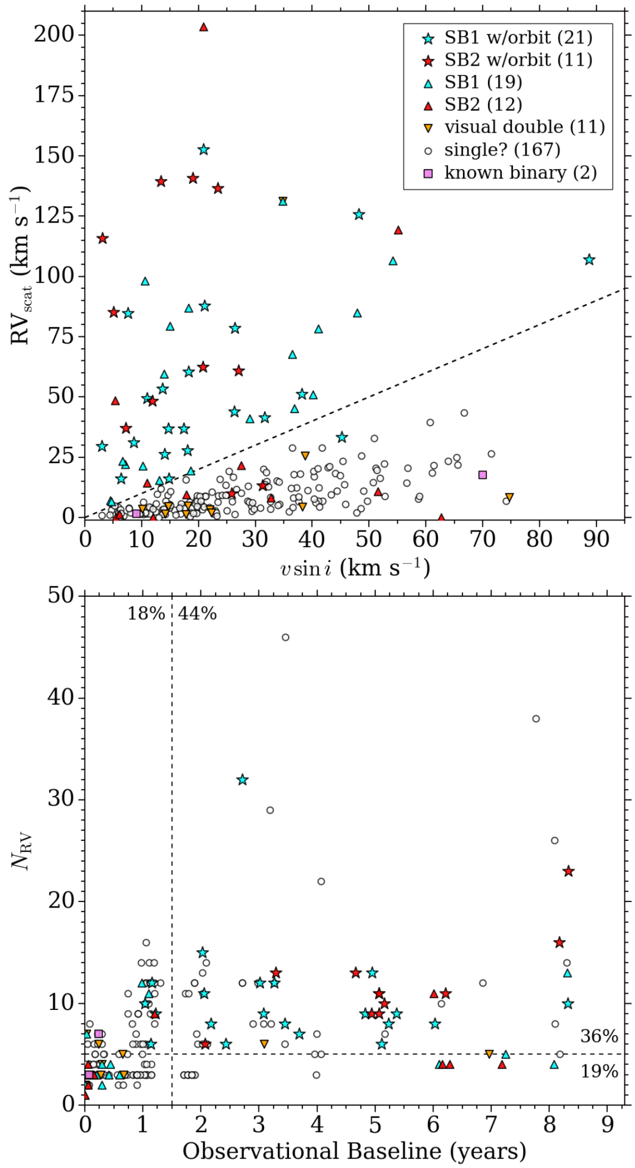

Figure 7. Top: Spectroscopic binary classification, whereby we consider everything with $RV_{scat} > v \sin i$ a definite binary or multiple, with a few exceptions. The dashed line indicates $RV_{scat} = v \sin i$. Bottom: Observational baseline versus number of RV measurements. The multiplicity fraction rises from 19 per cent to 45 per cent for stars with >1.5 yr observational baselines, and it rises from 20 per cent to 37 per cent for stars with more than five spectra.

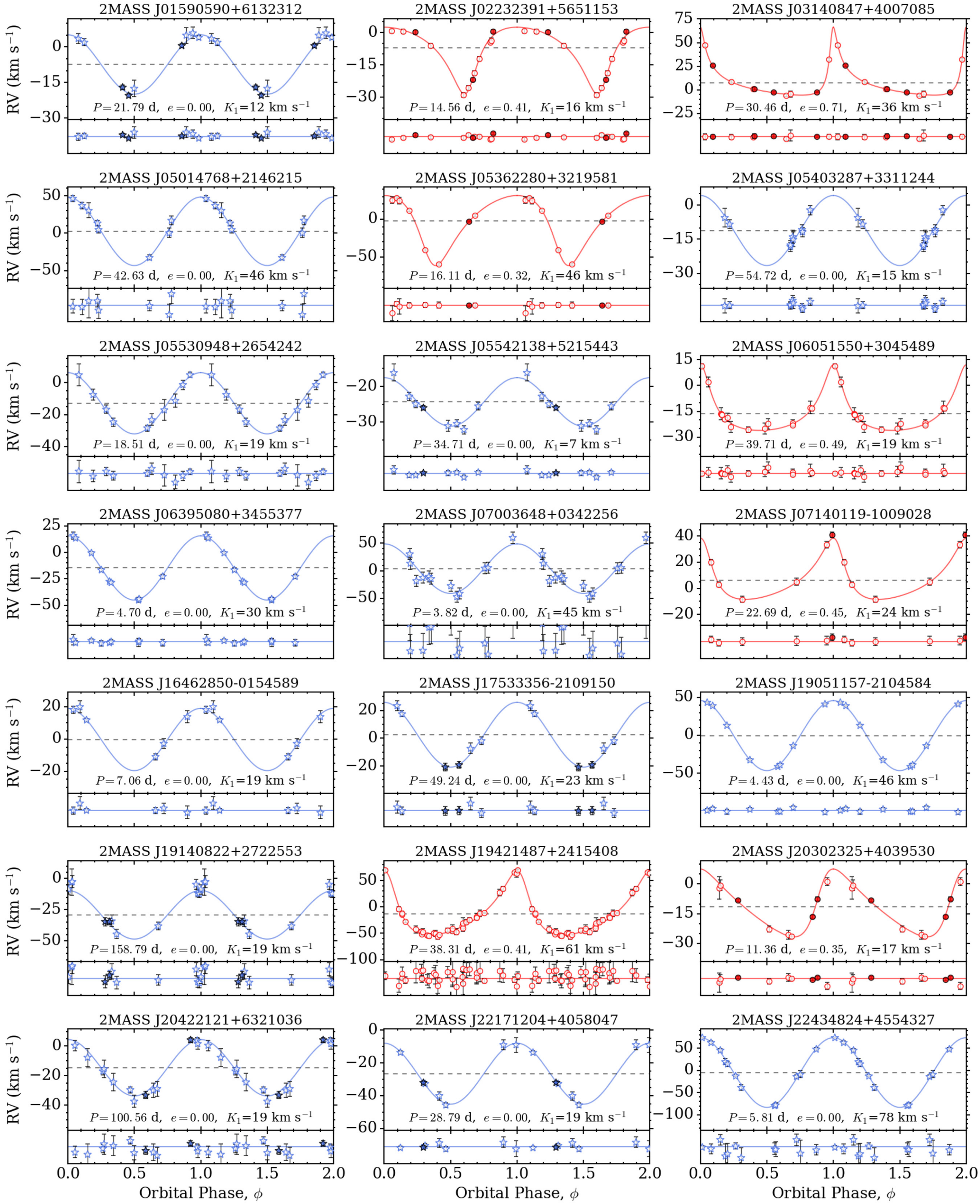

Figure 8. Orbital solutions for SB1s. The orbits have been repeated for two phases to improve the sense of continuity. The star symbols (blue) indicate circular orbits, circle symbols (red) indicate eccentric orbits, and filled symbols pertain to RV measurements from optical spectra. The dashed horizontal lines in the larger panels indicate the systemic velocities (γ), and solid lines are fits to the data. The smaller panels show the residuals of the observations minus the fit, with the ordinates covering $\pm 10\,\mathrm{km\,s^{-1}}$ and the horizontal lines indicating $y = 0$.

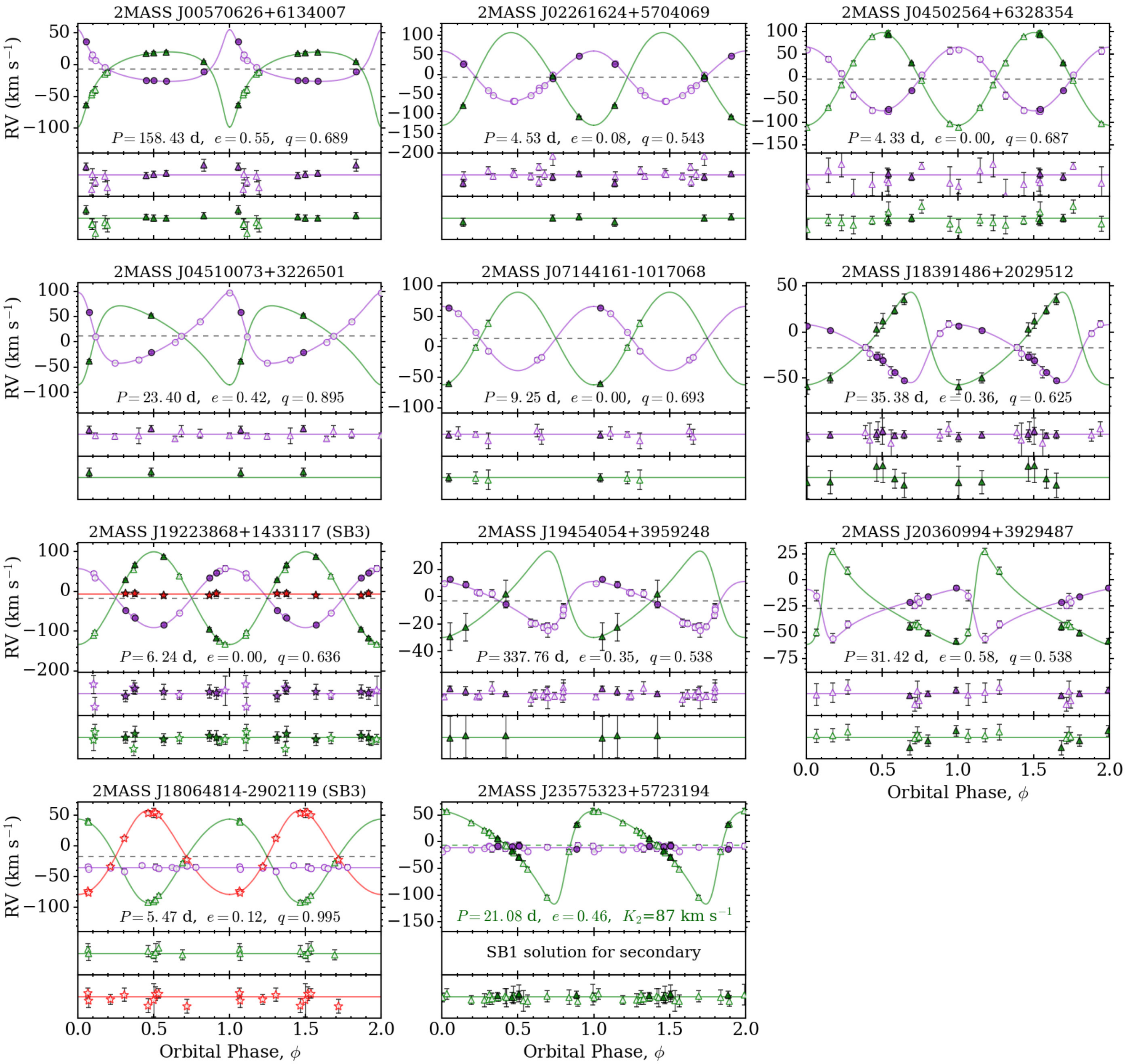

Figure 9. Orbital solutions for SB2s and multiple systems. The circle symbols (purple) are the RVs of the HgMn stars, triangle symbols (green) are the RVs of the secondary stars, star symbols (orange) are the RVs of the tertiary in the two SB3s, and filled symbols pertain to RV measurements from optical spectra. In the larger panels, dashed horizontal lines indicate the systemic velocity (γ), and if applicable, solid horizontal lines indicate the average RV of the binary component not included in the orbital solution. The smaller panels are as described in Fig. 8. For the SB3 2MASS J18064814−2902119, an SB2 orbital solution pertaining to the secondary (Ap) and tertiary (A/Am) components is shown, while for the SB3 2MASS J19223868+1433117, an SB2 orbital solution pertaining to the primary (HgMn) and tertiary (Am) components is shown. For 2MASS J23575323+5723194, an SB1 orbital solution pertaining to the Am component is shown.

often only becoming evident after smoothing the spectra. For Am stars, the Ce III lines are always significantly weaker than Mg I and Si I such that we do not expect to be able to distinguish a normal A-type companion from an Am companion in the APOGEE spectra of HgMn SB2s. The Ce III lines would likely be below our detection threshold. We therefore refer to the companions in these systems simply as ‘A/Am’ due to the ambiguity, but in reality it would not be surprising if the majority of the companions were indeed chemically peculiar stars.

On the other hand, at least 11 of the SB2 systems definitely involve chemically peculiar companions. This includes four cases of Ce III lines that are offset from Mn II, if not clearly varying in antiphase with respect to Mn II, and one case of multiple sets of Mn II lines in the APOGEE spectra. In another six cases, we classify the companions as Am stars based on detection of corresponding Sr II and Ba II lines in optical follow-up spectra (known to be overabundant for Am stars; see Ghazaryan, Alecian & Hakobyan 2018).

Table 6 summarizes the multilined systems, providing the companion types and $v \sin i$ along with the mass ratios for systems with orbital solutions, and Mg II 4481 Å flux ratios for systems with optical spectra. For systems with optical spectra in which

Table 4. Orbital solutions for SB1s.

2MASS ID	N_{RV}	P (d)	$T_{max,RV}$ (HJD-2.45E5)	e	ω (deg.)	γ (km s^{-1})	K_1 (km s^{-1})	$a_1 \sin i$ (AU)	$f[M_1, M_2]$ (M$_\odot$)	χ^2
01590590+6132312	9	21.794 ± 0.007	5791.904 ± 0.864	0.000 ± 0.000	90.000 ± 0.000	−7.416 ± 0.402	12.480 ± 0.611	0.025 ± 0.001	0.004 ± 0.001	6.081
02232391+5651153	12	14.565 ± 0.001	5805.879 ± 0.235	0.413 ± 0.031	201.647 ± 3.774	−7.098 ± 0.379	15.514 ± 0.517	0.019 ± 0.001	0.004 ± 0.001	17.423
03140847+4007085	10	30.456 ± 0.003	5809.752 ± 0.056	0.720 ± 0.048	333.549 ± 4.412	7.462 ± 0.440	36.576 ± 5.721	0.071 ± 0.012	0.052 ± 0.029	1.909
05014768+2146215	8	42.634 ± 0.024	5798.451 ± 0.460	0.000 ± 0.000	90.000 ± 0.000	2.570 ± 1.647	45.705 ± 3.063	0.179 ± 0.012	0.422 ± 0.085	3.118
05362280+3219581	8	16.109 ± 0.001	5796.707 ± 0.113	0.323 ± 0.033	148.052 ± 3.275	−2.315 ± 0.730	46.344 ± 1.040	0.065 ± 0.002	0.141 ± 0.018	1.448
05403287+3311244	9	54.717 ± 0.141	5786.653 ± 3.092	0.000 ± 0.000	90.000 ± 0.000	−11.192 ± 1.024	15.389 ± 2.491	0.077 ± 0.013	0.021 ± 0.010	3.665
05530948+2654242	10	18.507 ± 0.024	5796.129 ± 1.485	0.000 ± 0.000	90.000 ± 0.000	−12.862 ± 0.856	19.105 ± 1.210	0.033 ± 0.002	0.013 ± 0.003	3.647
05542138+5215443	8	34.707 ± 0.016	5777.021 ± 1.069	0.000 ± 0.000	90.000 ± 0.000	−24.348 ± 0.568	6.800 ± 1.065	0.022 ± 0.003	0.001 ± 0.001	7.340
06051550+3045489	15	39.714 ± 0.030	5763.395 ± 0.829	0.488 ± 0.034	8.508 ± 6.811	−16.222 ± 0.506	18.975 ± 1.081	0.060 ± 0.004	0.019 ± 0.004	3.559
06395080+3455377	9	4.701 ± 0.000	5798.665 ± 0.037	0.000 ± 0.000	90.000 ± 0.000	−14.682 ± 0.645	30.296 ± 0.762	0.013 ± 0.000	0.014 ± 0.001	1.787
07003648+0342256	12	3.820 ± 0.001	5798.888 ± 0.088	0.000 ± 0.000	90.000 ± 0.000	3.773 ± 3.177	44.994 ± 4.977	0.016 ± 0.002	0.036 ± 0.012	13.570
07140119−1009028	6	22.690 ± 0.009	5784.093 ± 1.042	0.449 ± 0.052	32.023 ± 8.620	5.998 ± 1.342	23.531 ± 1.350	0.044 ± 0.003	0.022 ± 0.006	2.642
16462850−0154589	6	7.056 ± 0.006	5799.671 ± 1.200	0.000 ± 0.000	90.000 ± 0.000	−0.303 ± 1.117	19.308 ± 2.442	0.013 ± 0.002	0.005 ± 0.002	1.546
17533356−2109150	6	49.240 ± 0.056	5770.478 ± 1.871	0.000 ± 0.000	90.000 ± 0.000	2.490 ± 1.749	23.324 ± 2.371	0.106 ± 0.011	0.065 ± 0.020	1.876
19051157−2104584	8	4.433 ± 0.000	5800.286 ± 0.082	0.000 ± 0.000	90.000 ± 0.000	−0.495 ± 0.377	46.238 ± 0.549	0.019 ± 0.000	0.045 ± 0.002	5.314
19140822+2722553	11	158.794 ± 0.379	5691.573 ± 4.639	0.000 ± 0.000	90.000 ± 0.000	−29.031 ± 1.510	19.420 ± 1.766	0.283 ± 0.026	0.121 ± 0.033	8.389
19421487+2415408	32	38.311 ± 0.013	5776.054 ± 0.298	0.412 ± 0.013	34.338 ± 2.492	−13.234 ± 0.550	60.766 ± 0.922	0.195 ± 0.003	0.673 ± 0.043	17.433
20302325+4039530	9	11.355 ± 0.002	5800.405 ± 0.519	0.346 ± 0.053	290.022 ± 2.155	−11.637 ± 0.427	17.125 ± 0.420	0.017 ± 0.001	0.005 ± 0.001	8.539
20422121+6321036	13	100.563 ± 0.171	5748.877 ± 3.348	0.000 ± 0.000	90.000 ± 0.000	−14.690 ± 0.969	19.122 ± 0.966	0.177 ± 0.009	0.073 ± 0.011	9.678
22171204+4058047	7	28.792 ± 0.012	5794.822 ± 1.176	0.000 ± 0.000	90.000 ± 0.000	−26.608 ± 1.170	18.614 ± 0.831	0.049 ± 0.002	0.019 ± 0.003	3.180
22434824+4554327	12	5.808 ± 0.000	5799.736 ± 0.056	0.000 ± 0.000	90.000 ± 0.000	−4.978 ± 1.057	78.317 ± 1.228	0.042 ± 0.001	0.289 ± 0.014	6.719

the companion lines were sufficiently separated from the primary lines, the companion $v \sin i$ estimates were determined using the *iacob broad* code. Otherwise, the calibration presented in Fig. 7 was used. In many cases, the binary components have nearly or definitely identical $v \sin i$, and in only three cases do we find one or more components with $v \sin i > 30$ km s^{-1}.

As noted in Section 6, the companion stars of four SB2s were detected in the optical but not in the *H*-band. Two of these companions are late-B, rapid rotators, such that we would not expect to see corresponding metal lines in the *H*-band (see the upper two spectra in Fig. 2.) Another two of the optical SB2s have cool, faint companions whose *H*-band lines are apparently too weak for detection in APOGEE spectra. Hence, although no convincing evidence is found for lines from companion star(s) in the APOGEE spectra of the SB1s represented in Fig. 8, optical spectroscopy will undoubtedly reveal additional SB2s among them, with companions that are too faint, hot, or rapidly rotating to be detected in the *H*-band.

In the following, we discuss the SB2 and SB3 systems individually.

6.3 Binaries with HgMn or Ap/Bp companions

2MASS J00570626+6134007 = HD 5429 is the clearest available example of an HgMn + Ap/Bp binary, making it the second such system known in addition to HD 161701 (González et al. 2014). The Ce III lines from the secondary star are quite obvious in the five APOGEE spectra as are numerous lines in our five optical spectra of the system, allowing us to derive the orbital solution shown in Fig. 9. With $P = 159$ d and $e = 0.55$, this is one of the widest and most eccentric binaries of the APOGEE HgMn sample. The weakness of the He I lines from the companion in the optical spectra indicates that it is either an late-B or early-A type star, and this is also suggested by the mass ratio ($M_2/M_1 = 0.689$) obtained from the orbital solution. The orbit also suggests a minimum mass of 5.6 $M_\odot$ for the primary, which places it among the most massive HgMn stars.

Fig. 10 shows selected regions of the optical spectra, with the left-hand columns demonstrating that both stars produce the low-energy Mn II lines that are numerous in the optical, and with the right-hand column demonstrating that only the Ap/Bp star contributes to doubly ionized rare earth lines like Pr III and Nd III. The Hg II 3984 Å line of the HgMn primary is among the weakest of our optical sample (see Fig. 5), but it is certainly present and without a counterpart from the Ap/Bp star. Instead, the Fe II and Cr II lines of the Ap/Bp star are overly strong, further suggesting that it is a magnetic chemically peculiar star. **2MASS J02060290+5009136** is an SB2 with an Ap/Bp companion that is detected in Ce III 15961 Å in three of the four available APOGEE spectra. The stronger Ce III 16133 Å line is unfortunately blended with residuals from the strong airglow line at 16128 Å, such that we could only measure RVs and estimate $v \sin i$ based on Ce III 15961 Å. The spectra also only cover a short time-scale of 21 d, but none the less, the Ce III RVs are clearly anticorrelated with those of the Mn II lines, with Ce III going from −41 km s^{-1} to −21 km s^{-1} and with Mn II going from −34 km s^{-1} to −42 km s^{-1}. More spectra will be needed to determine the orbital parameters of the system and to confirm that is indeed another example of the rare HgMn + Ap/Bp binaries. **2MASS J09432220−5348264 = HD 298641** is the only available example of an HgMn + HgMn binary in which multiple sets of Mn II lines were detected in the APOGEE spectra. Fig. 11 shows the Mn II 15413, 15600, and 15620 Å lines from the three

Table 5. Orbital solutions for SB2s and SB3s.

2MASS ID	N_{RV}	P (d)	$T_{max.RV}$ (HJD-2.45E5)	e	ω (deg.)	γ (km s^{-1})	$K_{1,2}$ (km s^{-1})	$a_{1,2}\,sin\,i$ (AU)	$M_{1,2}\,sin\,i^3$ (M$_\odot$)	χ^2
00570626+6134007A	10	158.426 ± 0.085	5853.884 ± 1.769	0.551 ± 0.551	346.451 ± 2.515	− 7.448 ± 0.430	40.703 ± 2.886	0.495 ± 0.037	5.621 ± 0.978	29.580
00570626+6134007B	10	158.426 ± 0.085	5853.884 ± 1.769	0.551 ± 0.551	346.451 ± 2.515	− 7.448 ± 0.430	59.114 ± 3.998	0.718 ± 0.052	3.870 ± 0.649	29.580
02261624+5704069A	13	4.527 ± 0.000	5798.103 ± 0.071	0.080 ± 0.080	61.463 ± 4.823	− 6.705 ± 0.428	64.129 ± 0.436	0.027 ± 0.000	1.823 ± 0.056	19.628
02261624+5704069B	3	4.527 ± 0.000	5798.103 ± 0.071	0.080 ± 0.080	61.463 ± 4.823	− 6.705 ± 0.428	118.139 ± 1.548	0.049 ± 0.001	0.990 ± 0.020	19.628
04502564+6328354A	11	4.334 ± 0.000	5798.698 ± 0.019	0.000 ± 0.000	90.000 ± 0.000	− 4.634 ± 0.705	70.442 ± 1.548	0.028 ± 0.001	1.378 ± 0.043	21.919
04502564+6328354B	11	4.334 ± 0.000	5798.698 ± 0.019	0.000 ± 0.000	90.000 ± 0.000	− 4.634 ± 0.705	102.545 ± 1.214	0.041 ± 0.000	0.946 ± 0.040	21.919
04510073+3226501A	9	23.405 ± 0.002	5779.814 ± 0.217	0.417 ± 0.417	55.914 ± 1.786	11.356 ± 0.463	70.006 ± 0.765	0.137 ± 0.002	3.126 ± 0.288	12.952
04510073+3226501B	2	23.405 ± 0.002	5779.814 ± 0.217	0.417 ± 0.417	55.914 ± 1.786	11.356 ± 0.463	78.182 ± 3.372	0.153 ± 0.007	2.799 ± 0.154	12.952
07144161−1017068A	6	9.251 ± 0.004	5800.291 ± 0.845	0.000 ± 0.000	90.000 ± 0.000	13.587 ± 0.912	52.587 ± 2.503	0.045 ± 0.002	1.202 ± 0.175	1.275
07144161−1017068B	3	9.251 ± 0.004	5800.291 ± 0.845	0.000 ± 0.000	90.000 ± 0.000	13.587 ± 0.912	75.916 ± 4.876	0.065 ± 0.004	0.832 ± 0.096	1.275
18391486+2029512A	13	35.378 ± 0.013	5821.247 ± 1.349	0.357 ± 0.357	235.924 ± 7.275	−17.055 ± 0.966	31.385 ± 1.804	0.095 ± 0.006	1.000 ± 0.213	4.338
18391486+2029512B	6	35.378 ± 0.013	5821.247 ± 1.349	0.357 ± 0.357	235.924 ± 7.275	−17.055 ± 0.966	50.249 ± 4.562	0.153 ± 0.014	0.625 ± 0.099	4.338
19223868+1433117A	11	6.235 ± 0.000	5797.070 ± 0.026	0.000 ± 0.000	90.000 ± 0.000	−17.065 ± 0.593	74.187 ± 1.026	0.043 ± 0.001	2.744 ± 0.067	10.823
19223868+1433117B	5	...	...	...	...	...	...	...	...	...
19223868+1433117C	11	6.235 ± 0.000	5797.070 ± 0.026	0.000 ± 0.000	90.000 ± 0.000	−17.065 ± 0.593	116.634 ± 1.149	0.067 ± 0.001	1.745 ± 0.048	10.823
19454054+3959248A	16	337.756 ± 1.956	5810.319 ± 4.003	0.352 ± 0.352	243.553 ± 17.223	− 3.093 ± 0.703	16.937 ± 1.706	0.492 ± 0.071	2.115 ± 0.823	12.284
19454054+3959248B	3	337.756 ± 1.956	5810.319 ± 4.003	0.352 ± 0.352	243.553 ± 17.223	− 3.093 ± 0.703	31.467 ± 3.093	0.914 ± 0.130	1.139 ± 0.428	12.284
20360994+3929487A	9	31.422 ± 0.012	5774.023 ± 0.576	0.582 ± 0.582	112.929 ± 3.548	−27.390 ± 0.666	23.770 ± 1.990	0.056 ± 0.005	0.358 ± 0.057	11.305
20360994+3929487B	9	31.422 ± 0.012	5774.023 ± 0.576	0.582 ± 0.582	112.929 ± 3.548	−27.390 ± 0.666	44.203 ± 2.145	0.104 ± 0.006	0.192 ± 0.036	11.305
18064814−2902119A	11	...	...	...	...	...	...	...	...	
18064814−2902119B	7	5.469 ± 0.000	5789.682 ± 0.210	0.116 ± 0.116	151.162 ± 8.748	−17.647 ± 0.793	68.402 ± 1.515	0.034 ± 0.001	0.707 ± 0.034	7.216
18064814−2902119C	9	5.469 ± 0.000	5789.682 ± 0.210	0.116 ± 0.116	151.162 ± 8.748	−17.647 ± 0.793	68.402 ± 1.515	0.034 ± 0.001	0.704 ± 0.031	7.216
23575323+5723194A	23	...	...	...	...	...	...	...	...	...
23575323+5723194B	23	21.080 ± 0.001	5806.240 ± 0.084	0.456 ± 0.456	234.674 ± 1.625	− 7.197 ± 0.930	86.620 ± 2.911	0.149 ± 0.005	...	4.260

Table 6. Summary of double-lined and triple-lined spectroscopic binaries. Mass ratios ($q = M_2/M_1$) are given for the systems with orbital solutions, and flux ratios (F_2/F_1) of Mg II 4481 Å are given for the systems with optical spectra. The v sin i [1], v sin i [2], and v sin i [3] columns give rotational velocity estimates for the primary, secondary, and tertiary stars where applicable and where possible to make such estimates.

2MASS Designation	Companion Type(s)	Orbital Period (days)	Mass Ratio (M_2/M_1)	Mg II Ratio (F_2/F_1)	v sin i [1] (km s^{-1})	v sin i [2] (km s^{-1})	v sin i [3] (km s^{-1})	Note
09432220−5348264	HgMn	...	...	...	5 ± 5	5 ± 5	...	...
19223868+1433117	BpMn, Am	6.2	0.636	0.967, 0.438	18 ± 2	17 ± 2	22 ± 5	SB3; SB2 orbit for HgMn + Am components
00570626+6134007	Ap/Bp	158.4	0.689	0.245	20 ± 1	8 ± 2	...	...
02060290+5009136	Ap/Bp	...	...	...	34 ± 4	29 ± 10	...	...
18064814−2902119	Ap/Bp, A/Am	...	...	...	26 ± 5	14 ± 6	15 ± 5	SB3; SB2 orbit for Ap + A/Am components
02261624+5704069	Am	4.5	0.543	0.203	3 ± 1	4 ± 1	...	companion not detected in *H*-band
04502564+6328354	Am	4.3	0.687	0.352	22 ± 2	16 ± 3	...	...
05380741+2418520	Am	...	...	0.271	58 ± 3	15 ± 4	...	...
07144161−1017068	Am	9.3	0.694	0.328	6 ± 3	6 ± 3	...	...
17314436−2616112	Am	...	...	0.134	3 ± 1	13 ± 2	...	...
20360994+3929487	Am	31.4	0.536	0.115	13 ± 2	11 ± 3	...	...
23575323+5723194	Am	...	...	0.227	33 ± 2	11 ± 1	...	...
04510073+3226501	late-B	23.4	0.895	1.100	13 ± 2	10 ± 3	...	companion not detected in *H*-band
18391486+2029512	late-B	35.4	0.625	0.787	25 ± 7	70 ± 10	...	companion not detected in *H*-band
19454054+3959248	late-B	337.8	0.538	∼1	9 ± 1	∼200	...	companion not detected in *H*-band
02203397+6023494	A/Am	...	...	...	27 ± 10	16 ± 7	...	multiple system?
04315476+2138086	A/Am	...	...	...	62 ± 8	62 ± 15	...	...
06402199−0322092	A/Am	...	...	...	51 ± 9	23 ± 7	...	multiple system? Long-period SB2?
06561603−2839053	A/Am	...	...	...	9 ± 4	22 ± 5	...	...
06572439−0928136	A/Am	...	...	...	28 ± 4	15 ± 6	...	...
14482274−5959316	A/Am	...	...	...	21 ± 11	18 ± 9	...	...
16133258−6019519	A/Am	...	...	...	11 ± 4	...	...	tentative detection in all APOGEE spectra
19294384−1801510	A/Am	...	...	...	12 ± 5	18 ± 7	...	...

spectra, with vertical lines denoting the lines from each star. The components were fully blended on MJD 58178 but well separated on MJDs 58181 and MJD 58206. Although the spectra in Fig. 11 are shown in the rest frame of the star that produces stronger Mn II 15413 Å, it is in fact the slightly more RV-variable star (RV$_{\rm scat}$ of 48.6 km s^{-1} versus 46.2 km s^{-1}). Based on the available data, it appears likely that the orbital period is less than 50 d.

2MASS J18064814−2902119 = HD 165347 is a known visual double star with a far fainter companion (5 magnitudes fainter) separated by 6.85 arcsec (Mason et al. 2001). The 11 APOGEE spectra of the system instead indicate that it is at least an SB3. One of the companions is an Ap/Bp star whose Ce III lines and *UL* (Ce III 15961 Å being the strongest line) are detected in 9/11 spectra, and the other is an A/Am star whose *NSL* (Si I 15964 Å being the strongest line) are detected in 7/11 spectra. The dominant component of the spectra is of course the HgMn star, but over the 6.2 yr observational baseline, the Mn II RVs vary by just 10 km s^{-1} with an average of −35 km s^{-1}. The Ap/Bp and A/Am stars are highly RV-variable however, with RV$_{\rm scat}$ of 130 and 133 km s^{-1}, respectively. Fig. 9 shows an SB2 orbital solution that suggests they are on a slightly eccentric orbit with $P = 5.47$ d and that the A/Am star is slightly more massive than the Ap/Bp star. The fact that the systemic velocity of the tight SB2 differs from the average RV of the HgMn star by almost 18 km s^{-1} may imply that the HgMn star is on a very long period orbit around either the inner SB2 or a fourth object.

2MASS J19223868+1433117 = HD 231263 is one of the more remarkable discoveries presented here. It is a known visual double star with a companion of comparable brightness (∼0.2 magnitude difference) that is separated by just 0.5 arcsec (Mason et al. 2001). This may be the Am SB2 companion that is detected in C I 16895 Å and the Mg I lines (15753, 15770 Å) in the six APOGEE spectra, but our five optical spectra of the system show that it is actually a multiple system composed of at least three stars. The third star apparently does not produce any strong lines in the *H*-band.

All three stars in the HD 231263 system produce Mg II, Si II, Ti II, Fe II, O I, and Balmer series lines in the optical, and detection of multiple sets of He I lines indicates that the secondary (undetected in the *H*-band) is a late-B type star. Simultaneous detection of Mn II lines (though not Hg II) at the right RVs further indicates that this late-B companion is in fact also an Mn-peculiar star, such that this is an HgMn+Bp Mn + Am system. However, it was the cooler tertiary that was detected in the APOGEE spectra and that is on a circular orbit around the HgMn star. Fig. 9 shows the associated SB2 orbital solution, which has a relatively short period of just ∼6.2 d.

Fig. 12 shows an attempt to de-blend the O I triplet lines using three sets of Gaussians with fixed equivalent width ratios based on the expected relative strengths of the lines. For the HgMn star, W(7772 Å) was fixed to the value measured from the apparently unblended line on MJD 58696, while for the Am star ('C'), W(7772 Å) was fixed to the average value measured from the apparently unblended lines on MJDs 58673 and 58767. For the Bp Mn star ('B'), the O I wavelengths and widths were fixed based on measurements of Fe II, Si II, and Mg II lines bluewards of H α, and the equivalent widths were simply adjusted until a satisfactory fit of the full blend was achieved. This resulted in W(7772 Å) of 90, 48, and 43 mÅ for the A, B, and C components, respectively.

The RVs of the Bp Mn star vary by just 4.7 km s^{-1} over the 109 d covered by the optical spectra, but the average RV of −7.3 km s^{-1} is quite close to the −17.1 km s^{-1} systemic velocity of the HgMn + Am SB2. It may be the case that the Bp Mn star is on a long period orbit around a fourth star, but it is certainly associated with the SB2.

6.4 Binaries with Am companions

2MASS J02261624+5704069 = HD 14900 is a known visual double star, with a far fainter companion (4.1 magnitudes fainter)

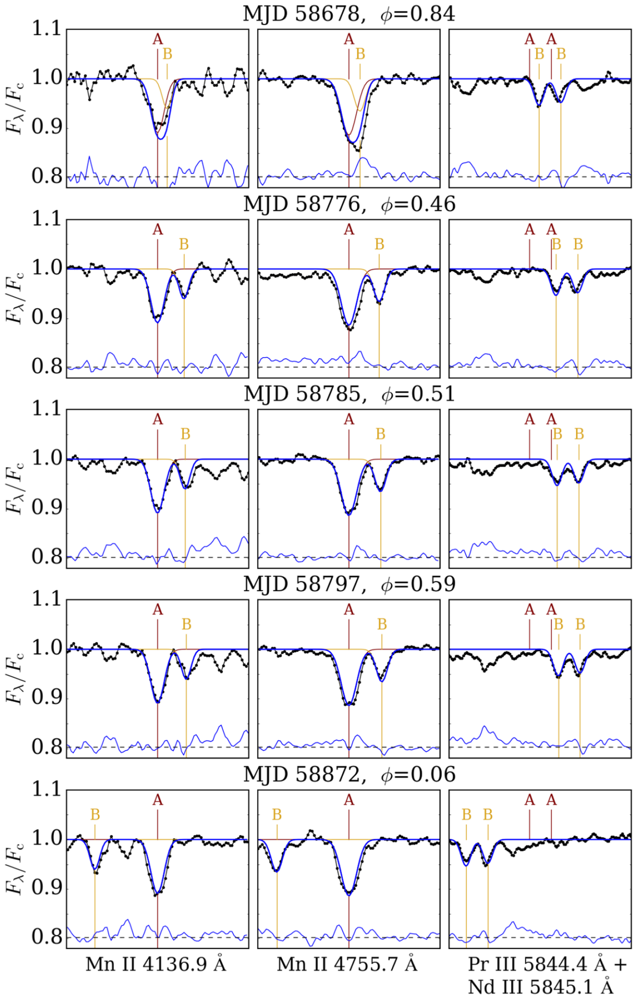

Figure 10. Optical spectra of the HgMn+Ap/Bp binary 2MASS J00570626+6134007 (HD 5429), highlighting the Mn II lines that are produced by both stars and the rare earth lines (e.g. Pr III and Nd III) that are produced by the Ap star (B) but not by the HgMn star (A). The spectra are shown in the rest frame of the HgMn star, and with individual Gaussians fits to the lines of each star (red and orange) as well as the sum of contributions from both stars (blue). Residuals are shown along the bottom of each panel, shifted upward artificially with the dashed lines indicating $y = 0$. The quoted orbital phases pertain to the orbital solution shown in Fig. 9.

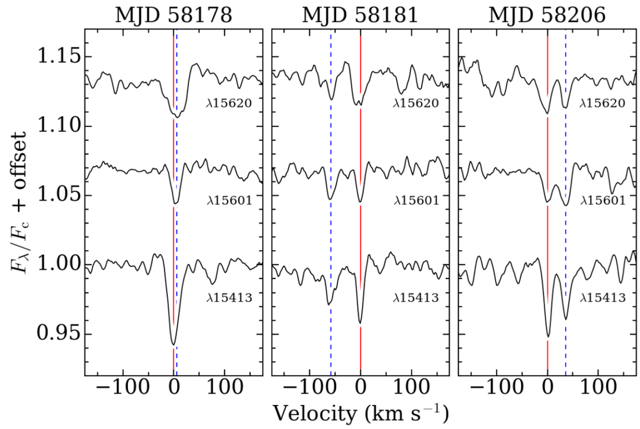

Figure 11. Multiple sets of Mn II lines in the *H*-band spectra of the SB2 2MASS J09432220−5348264 (HD 298641). The Mn II 15413, 15601, and 15620 Å line profiles are shown in the rest frame of the star with stronger Mn II, with a vertical dashed line indicating the position of the secondary star lines.

separated by 13 arcsec (Mason et al. 2001). Although we initially classified this system as an SB1, having found a short orbital period of 4.5 d based on the 10 APOGEE spectra, the companion was clearly detected in three subsequent optical spectra. The strongest line for the companion is Mg II 4481 Å ($W_\lambda = 24$ mÅ), but the Ba II resonance line at 4554 Å is of comparable strength ($W_\lambda = 14$ mÅ), suggesting that the companion is probably an Am star. Both stars are extremely slow rotators with $v \sin i \sim 3$–$4\,\mathrm{km\,s^{-1}}$. The orbital solution shown in Fig. 9 indicates a mass ratio of $q = 0.542$, which is among the smallest of the SB2 systems discussed in this paper. This might explain the *H*-band non-detection of the companion. **2MASS J04502564+6328354** is an SB2 with an Am companion that is clearly detected in the Mg I lines and in C I 16895 Å in the nine available APOGEE spectra and in numerous lines in two optical spectra. An orbital solution of the system is shown in Fig. 9, indicating a short period of just 4.3 d and a mass ratio of 0.687. The lack of He I lines at the companion velocities in the two optical spectra confirms the associated A spectral type, and this is further supported by the companion's low-energy Mg I and Fe I lines that lack counterparts from the HgMn star. The SB2 components were well-separated on one of the optical epochs (see Fig. 4), allowing for unambiguous identification of number Cr II, Sr II, and Ba II lines from the companion that are quite strong compared to Mg II 4481 Å. For example, the flux ratio of Sr II 4078 Å/Mg II 4481 Å is about 0.4, such that the companion is almost certainly an Am star. **2MASS J05380741+2418520 = HD 37242** is an SB2 in which *NSL* from the Am companion were detected in just one of three APOGEE spectra, with the *NSL* being offset from the Mn II lines by $\sim$166 km s^{-1} on that epoch. The system was subsequently confirmed as an SB2 by an optical spectrum in which the companion contributions are quite obvious. As with the other SB2s discussed in this section, we classify the companion as an Am star on the basis of overly strong Sr II and Ba II lines. In this case, the equivalent width of the companion's Ba II 4554 Å line is nearly half that of Mg II 4481 Å. Unlike most of the SB2 systems discussed here, the companion ($v \sin i = 15\,\mathrm{km\,s^{-1}}$) is a far slower rotator than the HgMn star ($v \sin i = 58\,\mathrm{km\,s^{-1}}$). More spectra will be needed for a full orbital analysis, but based on the large velocity separations of the SB2 components during the two epochs where both were detected, the orbital period is likely to be very short. **2MASS J07144161−1017068** is SB2 with an Am companion whose *NSL* were detected in only two of the five APOGEE spectra. The system is relatively faint ($H = 10.366$) compared to most of the sample, such that the companion's weak lines are only discernible after considerable smoothing of the spectra. Our optical follow-up spectrum confirmed that the system is indeed an SB2, and also that the companion is probably an Am star based on clear detection of the Ba II lines. Both of the stars are extremely slow rotators, with nearly identical $v \sin i$ of $\sim$6 km s^{-1}. Despite only six total spectra, the orbital period was constrained to <10 d by the APOGEE spectra (separated by 17 d) in which the companion was detected. An orbital solution with $e = 0$ and $P = 9.25$ d is shown in Fig. 9. **2MASS J17314436−2616112 = HD 158704** is a previously known HgMn star identified as an SB2 by Dolk et al. (2003). It is a visual double star with a 0.35 arcsec separation (Mason et al. 1999) and a clear SB2 in both the optical and *H*-band. A third companion

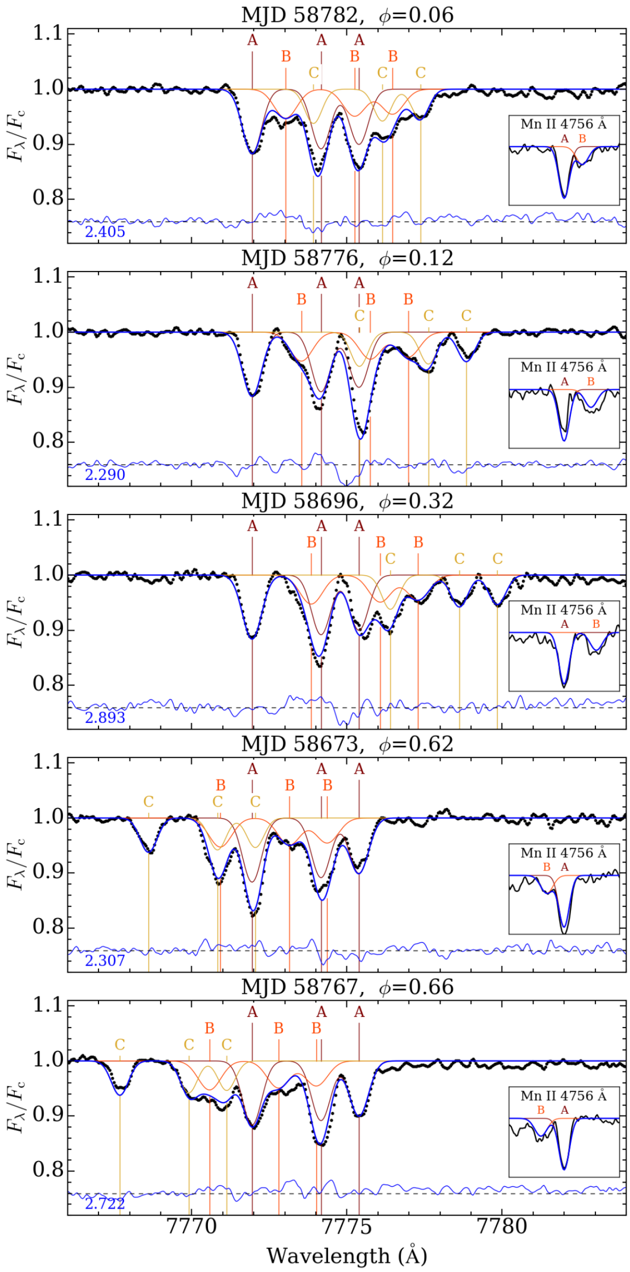

Figure 12. Optical spectra of the HgMn+Bp Mn+Am SB3 2MASS J19223868+1433117 (HD 231263), with the large panels showing the O I triplet (7772, 7774, 7775 Å) blend to which all three stars contribute and with the smaller panels showing an example of the Mn II lines that are produced by the HgMn (A) and Bp Mn (B) stars but not by the Am (C) star. Meanings are otherwise the same as in Fig. 10.

was identified in the high-contrast images presented by Schöller et al. (2010), and based on the relatively constant RVs (RV_{scat} of 5.7 km s^{-1} across 2 APOGEE spectra and 3 optical spectra) of the HgMn star, we suspect that this is indeed a multiple system. The slowly rotating Am companion is certainly RV-variable however, with RV_{scat} = 37.8 km s^{-1}. **2MASS J20360994+3929487** is one of the more obvious SB2s of the sample, with numerous narrow *NSL* detected in the six APOGEE spectra. The companion is a slowly rotating star with v sin $i\sim$11 km s^{-1}, and considering the relative weakness of its lines in the optical, it may be the coolest SB2 secondary of the sample. For example, attempts to deblend the contributions to Mg II 4481 Å from the two stars indicates that the companion line is perhaps only 10 per cent as strong the HgMn star line. Nonetheless, Ba II lines from the companion are clearly present in the spectra at strengths comparable to Mg II 4481 Å, such that we classify it as an Am star. Fig. 9 shows an orbital solution with a 31.4 d period and a relatively high eccentricity of $e = 0.58$. The mass ratio of $M_2/M_1 = 0.536$ is the lowest reported in this paper. **2MASS J23575323+5723194 = HD 224435** is another known visual multiple system, with at least two companions separated by 1.2 and 8.7 arcsec, respectively (Mason et al. 2001). The more distant companion is about 3.8 magnitudes fainter than the HgMn star, but the close companion is only 0.2 magnitudes fainter and hence is presumably the SB2 companion detected in the 18 APOGEE spectra and 4 optical spectra. The companion is a slow rotator with v sin $i\sim$11 km s^{-1} and with the Mg I and C I lines being the strongest *H*-band features. As with the other stars discussed in this section, we classify the companion as Am based on clear detection of Sr II and Ba II lines that are comparable in strength to Mg II 4481 Å. Despite the Am star being highly RV-variable, the RVs of the HgMn star vary by only $\sim$13 km s^{-1} over the 8.2 yr observational baseline, with variation pattern seeming unrelated to the motion of the Am star. Fig. 9 shows an SB1 orbital solution for the Am star, with the HgMn star RVs phased to the 21 d period. The average RV of the HgMn star is quite close to the systemic velocity indicated by the SB1 orbit of the Am star ($-$10.7 versus $-$7.2 km s^{-1}), such that the two stars are certainly associated.

6.5 Other SB2s and SB3s

2MASS J02203397+6023494 is a likely multiple system. The spectrum of an A/Am star was detected in all 11 APOGEE spectra, with the RVs varying by 11 km s^{-1}. The HgMn star RVs are even more highly RV-variable, with the maximum difference between epochs being 18 km s^{-1}. Despite this, we could not find reasonable orbital solutions for either star and certainly not for an SB2 combination since the relative RV variability seems random. **2MASS J04315476+2138086 = HD 28662** is a definite SB2 with an A or Am companion that is the fastest rotator (v sin $i\sim$62 km s^{-1}) of all the *H*-band-detected secondary stars described in this paper. In the single APOGEE spectrum of the system, the companion is most clearly detected in the Mg I lines between 15745–15770 Å and in C I 16895 Å, with those lines being offset from Mn II by roughly 149 km s^{-1}. **2MASS J04510073+3226501 = HD 30661** is another SB2 in which the companion was detected in optical spectra but not in the APOGEE spectra. An SB2 orbital solution shown in Fig. 9, and the associated mass ratio of $q = 0.895$ is the largest reported here. The optical data show that the stars are near spectroscopic twins in terms of almost identical v sin i and almost identical depths and strengths of the Balmer series, Si II, Fe II, Ti II, Mg II, and O I lines (among other species). The two most striking differences between the two stars are the lack of Mn II, Hg II, and other heavy metal lines from the companion star, as well as the relative strength of the He I lines for the two stars. Namely, the He I 5876 Å equivalent width of the HgMn star is about half that of the companion. This would normally suggest that the companion is in fact the hotter, more massive star, but in this case it is almost certainly due to a severe depletion of He for the HgMn star. **2MASS J06402199−0322092 = HD 47798** is a visual double star confirmed by Mason et al. (1999). We measured RVs from possible weak *NSL* features in the three APOGEE spectra covering 57 d, indicating that there may be an A/Am companion.

However, the resulting RVs are a good match to those of the HgMn star, with the averages being 22 and 23 km s^{-1}, respectively. The RV$_{\rm scat}$ is also small for both, at 5.5 km s^{-1} for the HgMn star and 2.5 km s^{-1} for the A/Am star. This may be a long-period SB2 or a multiple system. **2MASS J06561603−2839053 = HD 51459** is another SB2 with an A/Am companion. In the single APOGEE observation, the RVs of the HgMn and A/Am components were 65 and −79 km s^{-1}, respectively. Relatively strong Ce III lines (e.g, Ce III 15961 Å/Mn II 15413 Å ∼0.53) are present in the spectra, but their RVs and FWHM are all but identical to those of the Mn II lines. **2MASS J06572439−0928136 = HD 51539** is another SB2 with an A/Am companion that is clearly detected in the 3/4 available APOGEE spectra with sufficient S/N. The RVs of the HgMn and A/Am star vary by just 4.4 and 2.5 km s^{-1}, respectively, in the three spectra taken over 50 d, but the variability is anticorrelated. **2MASS J14482274−5959316 = HD 130039** was included in the sample due to fairly confident detection of Mn II 15413 and 15620 Å in the first of three APOGEE spectra (MJD 58657). That spectrum also exhibits numerous *NSL* (indicating an A/Am spectral type) at an RV of 98 km s^{-1} as compared to the Mn II RV of 0 km s^{-1}. The Mn II lines are not confidently detected in the subsequent two spectra (MJDs 56677 and 56689), but the A/Am star RVs drop to −23 km s^{-1} and then −133 km s^{-1} in those spectra. This is certainly an SB system, but it is unclear whether it actually involves an HgMn star. It is a known visual double star with a small separation of 0.56 arcsec, but the visual companion is 4.24 magnitudes fainter than the primary star (Horch et al. 2015). **2MASS J16133258−6019519** is a likely SB2 with an A/Am companion. The Mg I lines at 15753 and 15770 Å seem to definitely be present in the spectra, but disagreement of the RVs of the lines renders the result ambiguous. The HgMn star is only marginally RV-variable. **2MASS J18391486+2029512 = HD 172397** has a late-B SB2 companion that was detected in our five optical follow-up spectra but not in the seven APOGEE spectra. The *H*-band non-detection is almost certainly due in part to the relatively rapid rotation of the companion; based on fitting multiple Gaussians to the partially blended Si II 3863 Å, Mg II 4481 Å, and Fe II 5169 Å lines in one of the optical spectra, we estimate that the companion has v sin i∼70 km s^{-1}. Any *H*-band metallic features from the star would be quite weak to begin with, and probably undetectable for such a rapid rotator. The ratio of the equivalents of He I 4471 Å over Mg II 4481 Å for the companion is not much less than unity, indicating that it is definitely hotter than A0. The lack of detectable metal absorption features from the companion in the *H*-band is therefore unsurprising (see Fig. 2). Fig. 9 shows a possible SB2 orbit with a 35 d period and e = 0.36. **2MASS J19294384−1801510 = HD 183327** has an A/Am companion whose *NSL* are quite obvious and offset from the Mn II lines by ∼13 km s^{-1} in the single APOGEE spectrum. **2MASS J19454054+3959248 = HD 225692** has a broad-lined companion that was detected in our three optical spectra but not in the 13 APOGEE spectra. The broad components are most obvious in the He I lines and Mg II 4481 Å, with weaker contributions in the Si II and O I lines, indicating that it is a late-B type star. Based on attempts to fit Gaussians to the blended He I 4471 Å and Mg II 4481 Å region, we estimate that the companion has v sin i∼200 km s^{-1}. Thus, it is not terribly surprising that we see no evidence of this star in the APOGEE spectra, since it might not produce significant metal absorption lines even if it was not such a rapid rotator. The orbital solution shown in Fig. 9 indicates P = 338 d, which matches the period found if we treat the system as an SB1, and which is by far the longest orbital period reported in this paper. The mass ratio of the SB2 orbital solution

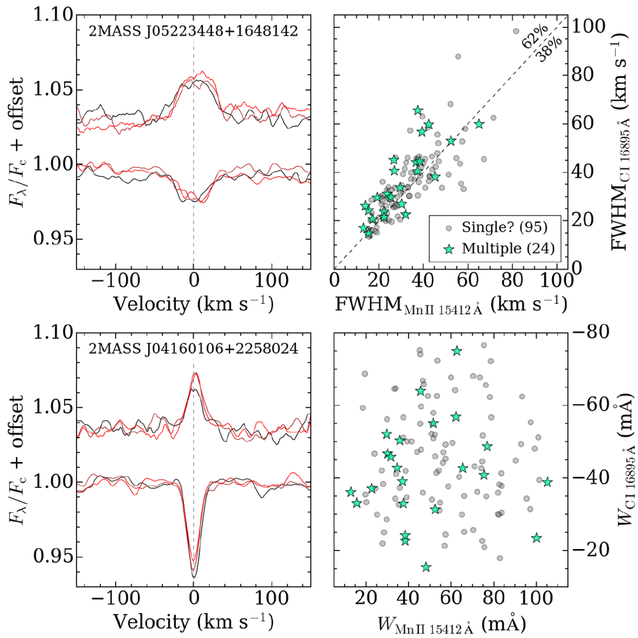

Figure 13. Left-hand panels: Demonstration of the matching radial velocities and line widths of Mn II 15413 Å absorption and C I 16895 Å emission. Each panel shows spectra from three epochs, corrected to rest frame based on the Mn II radial velocities and with the C I region artificially shifted upwards. 2MASS designations are given above each panel. Upper right-hand panel: The FWHMs of Mn II 15413 Å versus those of C I 16895 Å, with the dotted line indicating $y = x$. Lower right-hand panel: The equivalent widths of the same lines. The star symbols indicate binary and multiple systems.

(M_2/M_1 = 0.538) is among the lowest reported in this paper, which is surprising considering that the companion is a B-type star.

7 CARBON EMISSION

As mentioned in Section 3 and Fig. 2, HgMn stars often exhibit conspicuous narrow emission in the C I 16895 Å line. More specifically, this is true for roughly 45 per cent of the sample (120 stars). Only in cases of exceptionally strong C I 16895 Å emission are the weaker C I lines at 16009 and 16026 Å (labelled in Fig. 2) observed in emission. To confirm that the emission is in fact associated with the HgMn stars rather than being some kind of spurious artefact, we fit Gaussians to the C I emission features in order to obtain estimates of the RV, FWHM, and equivalent width of the feature.

Based on this, our first conclusion regarding the nature of the line emission is demonstrated in the two left-hand panels of Fig. 13. These panels show the Mn II 15413 Å (lower lines) and C I 16895 Å (upper lines) line profiles from three epochs for two stars that exemplify the behaviour of these lines. The spectra have been shifted to rest frame based on the RVs of the Mn II lines, making it clear that the C I emission occurs at roughly the same RVs is therefore definitely associated with the HgMn stars. However, small blueshifts (1–5 km s^{-1}) of the C I emission peaks are visible in most of the displayed spectra, indicating that the emission forms just above the surfaces of the stars.

Our second conclusion is the one made obvious by inspection of the line profile widths in left-hand panels of Fig. 13, and then quantified in the upper right-hand panel, which plots the FWHM of the C I 16895 Å emission versus the FWHM of Mn II 15413 Å. There is considerable scatter about the $y = x$ line, with 62 per cent of the stars having C I wider than Mn II, but the suggestion is none the less that the C I emission exhibits the same level of broadening as the Mn II lines and is therefore definitely associated with the surfaces of the stars. The same conclusions were reached by Wahlgren & Hubrig (2000) with respect to narrow emission lines in the optical spectra of chemically normal and chemically peculiar late-B stars.

As far as correlations with other spectral features, there are none to be found in the APOGEE spectra. The lower right-hand panel of Fig. 13 plots the equivalents widths of Mn II 15413 Å versus those of C I 16895 Å, showing that the strength of the C I emission has no dependence on the strength of the Mn II absorption lines. There also does not seem to be a correlation between C I emission and binarity, since the fraction of stars with C I emission that are definitely binaries or multiples (20 per cent) is considerably lower than the 31 per cent binary fraction for the full sample.

Emission in the C I 16895 Å line is certainly not a rare phenomenon and is not limited to chemically peculiar stars; recall that the B8 V star HD 2559 exhibits C I emission in the spectrum shown in Fig. 2. C I emission is also present in ~20 per cent of the classical Be star spectra obtained by APOGEE (Chojnowski et al. 2015), and the emission is particularly strong in the case of exotic binaries such as Be + sdO (HD 55606; Chojnowski et al. 2018) and Be + black hole (HD 215227; Casares et al. 2014). The C I 16895 Å line is also observed in emission in the spectra of blue supergiants (e.g. HD 15266), pre-main-sequence, supergiant, and unclassified B[e] stars (e.g. MWC 361, MWC 137, and MWC 922), luminous blue variables (e.g. S Doradus), post-AGB stars (e.g. IRAS 05040 + 4820), and extreme Helium stars (e.g. V2244 Oph).

8 DISCUSSION

Thanks to the strategy of selecting as telluric standards thousands of blue stars across the sky down to $H = 11$, the APOGEE survey has more than doubled the known sample of HgMn stars, expanding it from ~194 stars to a grand total of just over 450 stars. Although still quite rare, we estimate that somewhere between 5 and 10 per cent of the late-B stars observed by APOGEE are in fact HgMn stars. This significant increase of the sample of HgMn stars promises to open new perspectives for our knowledge and understanding of mid to late-main sequence B-type stars, and some inferences can already be made based on the basic analysis presented in this paper.

Combining the 30 orbital solutions for new HgMn stars with the 40 orbital solutions for known HgMn stars in the 9th Catalogue of Spectroscopic Binary Orbits (Pourbaix et al. 2009), we have orbital period estimates for a total of 70 HgMn binaries. Of these systems, 57/70 (77 per cent) have periods less than 75 d, 54/70 (74 per cent) have periods less than 50 d, and 40/70 (57 per cent) have periods less than 25 d. This result is emphasized in the upper panel of Fig. 14, which shows that the distribution of orbital periods (excluding the 16 systems with $P > 75$ d) is strongly peaked in the 5–10 d range. The previously suggested preference for short orbital periods (Hubrig & Mathys 1995) is therefore confirmed.

The lower panel of Fig. 14 shows the distribution of v sin i for HgMn stars, confirming that HgMn stars are slow rotators as a rule. The overall average is $<v \sin i> = 28$ km s^{-1} and the distribution is strongly peaked towards $v \sin i \sim 20$ km s^{-1}. For comparison, the average v sin i of non-supergiant, B7–A0, apparently chemically normal stars included in the catalogue of Abt, Levato & Grosso (2002) is >120 km s^{-1}. The phenomenon of B-type stars exhibiting HgMn abundance anomalies is therefore intimately linked not only with their multiplicity but with their slow rotation. These are key ingredients in the formation of HgMn stars.

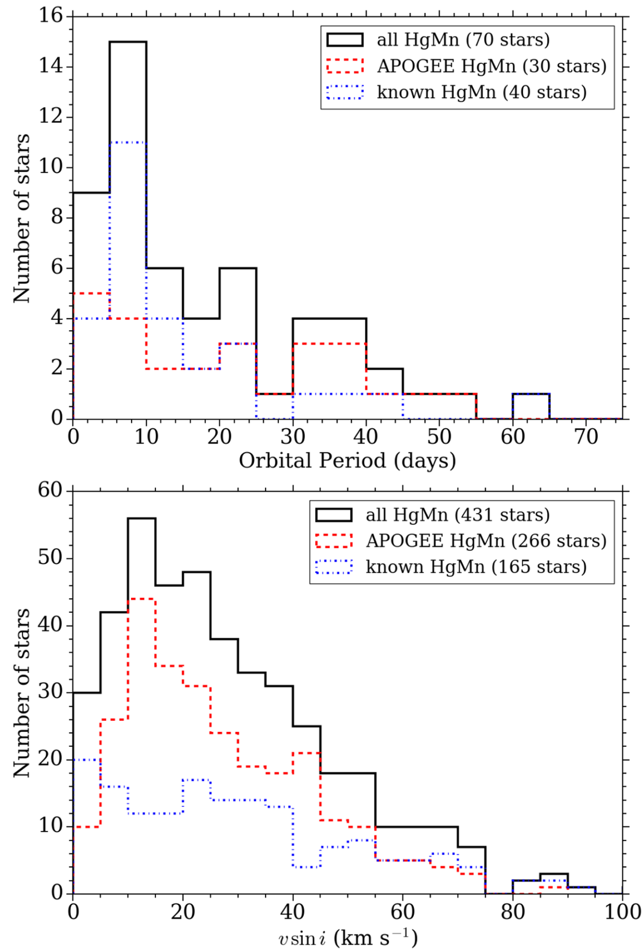

Figure 14. Histogram of orbital periods for HgMn binaries. The solid line indicates the APOGEE sample, and the dashed line indicates the known sample.

ACKNOWLEDGEMENTS

We dedicate this paper to the memory of Dr. Fiorella Castelli, whose contributions to the study of chemically peculiar stars will not be forgotten. We also thank the anonymous referee for useful comments that improved this paper.

Funding for the Sloan Digital Sky Survey IV has been provided by the Alfred P. Sloan Foundation, the U.S. Department of Energy Office of Science, and the Participating Institutions. SDSS acknowledges support and resources from the Center for High-Performance Computing at the University of Utah. The SDSS web site is www.sdss.org.

SDSS is managed by the Astrophysical Research Consortium for the Participating Institutions of the SDSS Collaboration including the Brazilian Participation Group, the Carnegie Institution for Science, Carnegie Mellon University, the Chilean Participation Group, the French Participation Group, Harvard-Smithsonian Center for Astrophysics, Instituto de Astrofísica de Canarias, The Johns Hopkins University, Kavli Institute for the Physics and Mathematics of the Universe (IPMU) / University of Tokyo, Lawrence Berkeley National Laboratory, Leibniz Institut fur Astrophysik Potsdam (AIP), Max-Planck-Institut fur Astronomie (MPIA Heidelberg), Max-Planck-Institut für Astrophysik (MPA Garching), Max-Planck-Institut für Extraterrestrische Physik (MPE), National Astronomical Observatories of China, New Mexico State University, New York University, University of Notre Dame, Observatório Nacional / MCTI, The Ohio State University, Pennsylvania State University, Shanghai Astronomical Observatory, United Kingdom Participation Group, Universidad Nacional Autónoma de México, University of Arizona, University of Colorado Boulder, University of Oxford, University of Portsmouth, University of Utah, University of Virginia, University of Washington, University of Wisconsin, Vanderbilt University, and Yale University.

Sten Hasselquist is supported by a National Science Foundation Astronomy and Astrophysics Postdoctoral Fellowship under award AST-1801940. D. A.García-Hernández acknowledges support from the State Research Agency of the Spanish Ministry of Science, Innovation and Universities and the European Regional Development Fund under grant AYA2017-88254-P.

REFERENCES

Abt H. A., Levato H., Grosso M., 2002, ApJ, 573, 359
Aguado D. S. et al., 2019, ApJS, 240, 23
Alecian G., Gebran M., Auvergne M., Richard O., Samadi R., Weiss W. W., Baglin A., 2009, A&A, 506, 69
Andrews J. J., Chanamé J., Agüeros M. A., 2017, MNRAS, 472, 675
Blanton M. R. et al., 2017, AJ, 154, 28
Bowen I. S., Vaughan A. H., 1973, Appl. Opt., 12, 1430
Briquet M., Korhonen H., González J. F., Hubrig S., Hackman T., 2010, A&A, 511, A71
Ćalıskan Ş., Ünal Ö., 2017, AIPC, 140001, AIPC.1815
Casares J., Negueruela I., Ribó M., Ribas I., Paredes J. M., Herrero A., Simón-Díaz S., 2014, Nature, 505, 378
Castelli F., Hubrig S., 2004, A&A, 425, 263
Chojnowski S. D. et al., 2015, AJ, 149, 7
Chojnowski S. D. et al., 2018, ApJ, 865, 76
Chojnowski S. D. et al., 2019, ApJ, 873, L5
Cowley C. R., Aikman G. C. L., 1975, PASP, 87, 513
Dolk L., Wahlgren G. M., Hubrig S., 2003, A&A, 402, 299
Eisenstein D. J. et al., 2011, AJ, 142, 72
Ghazaryan S., Alecian G., 2016, MNRAS, 460, 1912
Ghazaryan S., Alecian G., Hakobyan A. A., 2018, MNRAS, 480, 2953
González J. F., Levato H., 2009, Rev. Mex. Astron. Astrofis. Ser. Conf., 300, 35
González J. F. et al., 2014, A&A, 561, A63
Gunn J. E. et al., 2006, AJ, 131, 2332
Horch E. P., van Belle G. T., Davidson J. W., Ciastko L. A., Everett M. E., Bjorkman K. S., 2015, AJ, 150, 151
Hubrig S., Mathys G., 1995, Comments Astrophys., 18, 167
Hubrig S., Castelli F., Wahlgren G. M., 1999, A&A, 346, 139
Hubrig S. et al., 2010, MNRAS, 408, L61
Hubrig S. et al., 2012, A&A, 547, A90
Hubrig S. et al., 2014, MNRAS, 440, L6
Hubrig S., Järvinen S. P., Korhonen H., Ilyin I., Schöller M., Niemczura E., Chojnowski S. D., 2020, MNRAS, 495, L97
Hümmerich S., Niemczura E., Walczak P., Paunzen E., Bernhard K., Murphy S. J., Drobek D., 2018, MNRAS, 474, 2467
Iglesias-Marzoa R., López-Morales M., Jesús Arévalo Morales M., 2015, PASP, 127, 567
Kervella P., Arenou F., Mignard F., Thévenin F., 2019, A&A, 623, A72
Korhonen H. et al., 2013, A&A, 553, A27
Majewski S. R. et al., 2017, AJ, 154, 94
Makaganiuk V. et al., 2011, A&A, 529, A160
Makaganiuk V. et al., 2012, A&A, 539, A142
Malanushenko V. P., 1996, Ap, 39, 208
Mason B. D. et al., 1999, AJ, 117, 1890
Mason B. D., Wycoff G. L., Hartkopf W. I., Douglass G. G., Worley C. E., 2001, AJ, 122, 3466
Mathys G., Hubrig S., 1995, A&A, 293, 810
Monier R., Gebran M., Royer F., 2015, A&A, 577, A96
Monier R., Gebran M., Royer F., 2016, in Reylé C., Richard J., Cambrésy L., Deleuil M., Pécontal E., Tresse L., Vauglin I., eds, SF2A-2016: Proceedings of the Annual meeting of the French Society of Astronomy and Astrophysics, 14-17 June, 2016 at the Centre de Recherche Astrophysique de Lyon, p. 213
Monier R., Gebran M., Royer F., Kılıcoğlu T., 2017, in Reylé C., Di Matteo P., Herpin F., Lagadec E., Lançon A., Meliani Z., Royer F., eds, Proceedings of the Annual meeting of the French Society of Astronomy and Astrophysics, 4-7 July, 2017 in Paris, p. 45
Nidever D. L. et al., 2015, AJ, 150, 173
Pourbaix D. et al., 2004, A&A, 424, 727
Pourbaix D. et al., 2009, A&A, 424, 72
Renson P., Manfroid J., 2009, A&A, 498, 961
Ryabchikova T., 1998, in North P., Schnell A., Ziznovsky J., eds, Abundance Analysis of SB2 Binary Stars with HgMn Primaries , vol. 27. Contrib. Astr. Obs. Skalnate Pleso, Tatranská Lomnica, the Slovak Republic, p. 319.
Ryabchikova T. A., Malanushenko V. P., Adelman S. J., 1999, A&A, 351, 963
Schneider H., 1981, BICDS, 20, 113
Schöller M., Correia S., Hubrig S., Ageorges N., 2010, A&A, 522, A85
Simón-Díaz S., Herrero A., 2014, A&A, 562, A135
Skrutskie M. F. et al., 2006, AJ, 131, 1163
Smith K. C., Dworetsky M. M., 1993, A&A, 274, 335
Tsymbal V. V., Kotchukhov O. P., Khokhlova V. L., Lambert D. L., 1998, Astron. Lett., 24, 90
Wahlgren G. M., Hubrig S., 2000, A&A, 362, L13
Wang S.-i. et al., 2003, in Cameron D. G., ed., Proc. SPIE Conf. Ser. Vol. 1145, 7th Intl Conf on Fourier Transform Spectroscopy. SPIE, Bellingham, p. 4841
White R. E., Vaughan A. H., Preston G. W., Swings J. P., 1976, ApJ, 204, 131
Wilson J. C. et al., 2019, PASP, 131, 055001
Zasowski G. et al., 2013, AJ, 146, 81
Zasowski G. et al., 2017, AJ, 154, 198

SUPPORTING INFORMATION

Supplementary data are available at *MNRAS* online.

Table 1. Summary of the APOGEE HgMn sample.
Table 3. Radial velocity data.

Please note: Oxford University Press is not responsible for the content or functionality of any supporting materials supplied by the authors. Any queries (other than missing material) should be directed to the corresponding author for the article.

This paper has been typeset from a TEX/LATEX file prepared by the author.